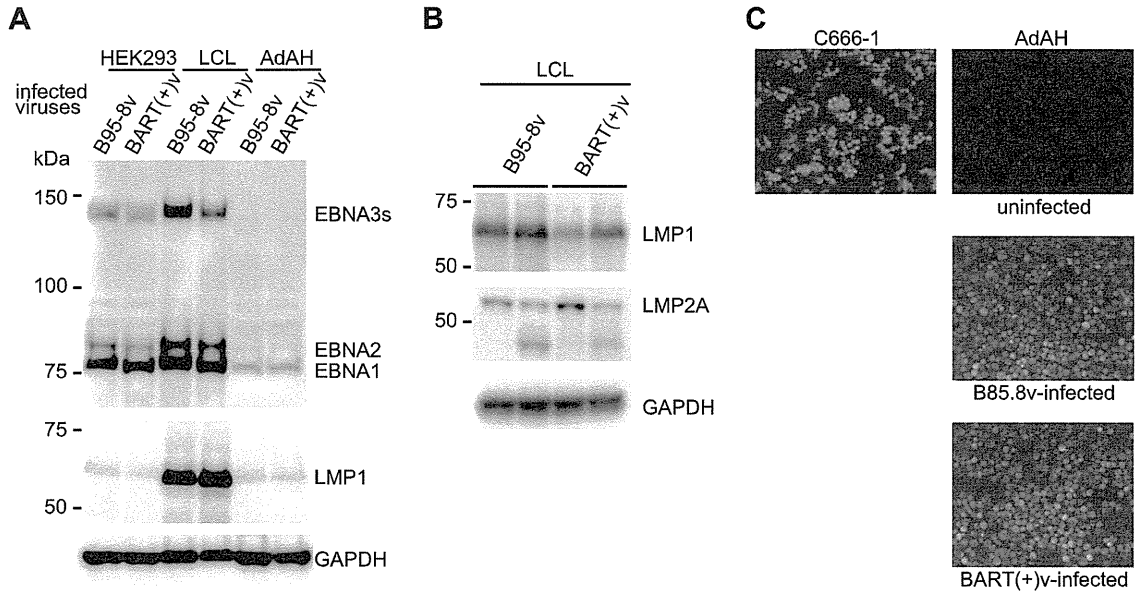

FIG 3 Immunoblot analyses of viral latent gene expression in cells infected with the recombinant viruses. (A) Whole-cell extracts of the B95.8v-infected and the BART(+)v-infected HEK293 cells, LCLs, and AdAH cells were analyzed by immunoblotting using EBV-immune human serum (top panel), a monoclonal anti-LMP1 antibody (middle panel), or an anti-GAPDH antibody (bottom panel) as a control. (B) LMP1 and LMP2A protein levels of two additional lines of the B95.8v-infected and the BART(+)v-infected LCLs were examined by Western blotting analyses. (C) The AdAH cells infected with the recombinant viruses were processed for immunofluorescence to detect the expression of EBNA. The EBNA staining of C666-1 is shown as a positive control.

examined cells (Fig. 2A and data not shown). Notably, the expression levels of the restored miRNAs were comparable to those of the endogenous miRNAs in the C666-1 cells, which express high levels of viral miRNAs (15).

Previous studies demonstrated that relative BART miRNA expression levels in LCLs were far less than those in epithelial cells (50), which was not very obvious in our Northern blot data. Thus, two of the BART miRNAs (BART17-5p and BART22) were chosen and subjected to TaqMan small RNA assay to determine miRNA expression levels in the BART(+)v-infected epithelial cells relative to those in the BART(+)v-infected LCLs. The results revealed that relative BART17-5p expression levels in the infected epithelial cells were comparable to those in the LCLs, whereas BART22 expression levels in BART(+)v-infected epithelial cells were approximately five times (HEK293 cells) and two times (AdAH cells) more than those in the BART(+)v-infected LCLs (Fig. 2B). These results were in good concordance with the Northern blot data, indicating that estimation of miRNA expression levels by Northern blotting data is reliable.

Whole-cell extracts were prepared from various B95.8v-infected and BART(+)v-infected cells (HEK293, LCLs, and AdAH cells), and the expression levels of viral latent proteins were examined by immunoblotting. The Epstein-Barr virus nuclear antigen 1 (EBNA1), EBNA2, and EBNA3 proteins were expressed at comparable levels in B95.8v-infected and BART(+)v-infected HEK293 cells and LCLs (Fig. 3A). Latent membrane protein 1 (LMP1) and LMP2A were expressed in the LCLs, but their expression levels were highly variable among different LCL cell clones (Fig. 3A and B). Thus, the effect of BART miRNA expression on LMP1 and LMP2A expression was obscure in this experimental setting. Although only traces of EBNA1 and LMP1 were detected by Western blotting, the infected AdAH cells were nearly 100% EBNA-positive (Fig. 3C), arguing against the possibility that only minor populations of AdAH cells were infected. These results indicate that the absence or presence of BART miRNAs did not significantly affect viral latent protein expression.

NDRG1 is downregulated in the cells infected with the BART-restored EBV. Next, microarray analyses were performed to identify differences between the expression levels of host genes in the B95.8v-infected and the BART(+)v-infected HEK293 cells (see Dataset S1 in the supplemental material). Two independent B95.8v-infected and two independent BART(+)v-infected HEK293 cell clones, each of which were derived from a single colony after hygromycin selection, were chosen based on their good virus producing abilities. Representative scatter plots of the global gene expression profiles of the B95.8v-infected and the BART(+)v-infected HEK293 cells are shown in Fig. 4A. We focused on cellular genes that were downregulated in the BART(+)v-infected HEK293 cells, since these genes are more likely to be direct targets of the EBV BART miRNAs. The analysis identified 19 genes that were expressed at moderate to high levels in the B95.8v-infected HEK293 cells and downregulated (0.75-fold or less) in the BART(+)v-infected HEK293 cells (see Table S5 in the supplemental material). We then used the DIANA-microT program (51) to search for possible direct target genes of each BART miRNA. Of the downregulated genes shown in Table S5 in the supplemental material, *NDRG1*, *NOM1*, and *ANGEL2* were identified as possible direct targets of BART miRNA (see Dataset S2 in the supplemental material). *NDRG1* (N-myc downstream regulated gene 1) was chosen for further analyses, because the gene had previously been identified as a BART miRNA target by a photoactivatable-ribonucleoside-enhanced cross-linking and immunoprecipitation analysis (32). NDRG1 mRNA expression was downregulated in the BART(+)v-infected AdAH cells as well (Fig. 4A and see Table S6 in the supplemental material). The downregulation of *NDRG1* expression in the BART(+)v-infected HEK293 cells was confirmed by quantitative RT-PCR (Fig. 4B).

Whole-cell extracts were prepared from B95.8v-infected and

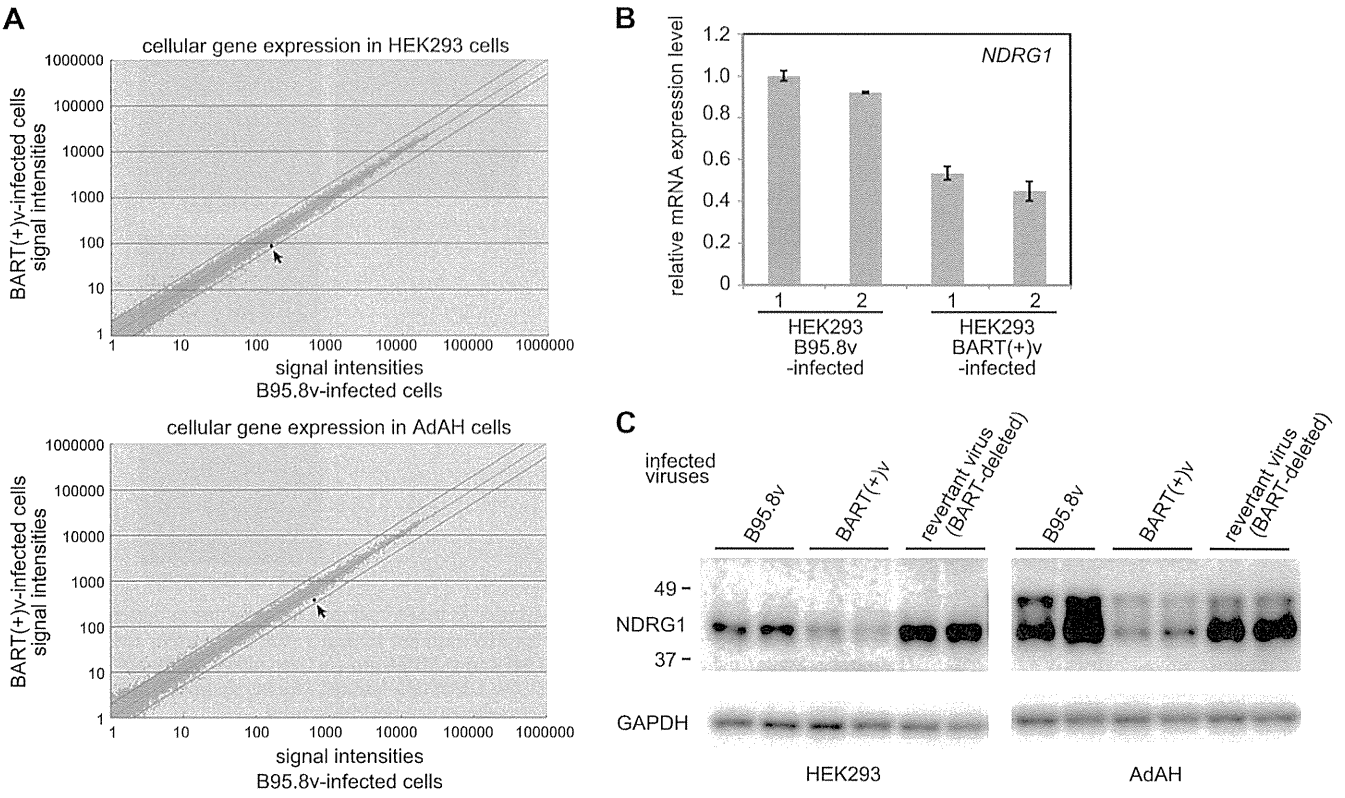

FIG 4 Downregulation of NDRG1 mRNA and protein in epithelial cells infected with the BART-restored virus. (A) Representative scatter plots of the global gene expression profiles of the B95.8v-infected and the BART(+)v-infected HEK293 and AdAH cells. The black dots (indicated by arrows) represent *NDRG1*, and the top and bottom diagonal lines indicate 2-fold differences between the expression levels in the two samples. The signal intensities of selected genes, including *NDRG1*, are shown in Tables S5 and S6 in the supplemental material. (B) Quantitative RT-PCR analyses of the expression levels of *NDRG1* mRNAs in the B95.8v-infected and the BART(+)v-infected HEK293 cells (two independent clones of each). The values were normalized by using those of *GAPDH* mRNA. The data are represented as the means ± the standard deviations (SD) of $n = 3$ replicates. (C) Immunoblot analyses of NDRG1 and GAPDH protein levels in whole-cell extracts of the B95.8v-infected cells, the BART(+)v-infected cells, and the revertant virus-infected cells (HEK293 and AdAH cells, two independent clones of each).

BART(+)v-infected HEK293 and AdAH cells, and the expression levels of the NDRG1 protein were examined by immunoblotting. In agreement with the mRNA levels, NDRG1 protein expression was downregulated in the BART(+)v-infected HEK293 cells (Fig. 4C). To confirm that the 12-kb region of EBV that is deleted in the B95-8 strain is responsible for downregulating NDRG1 expression, this region was removed from the BART(+) EBV-BAC clone to generate a BART-deleted revertant. An immunoblot analysis revealed that HEK293 stably infected with the revertant virus exhibited high levels of NDRG1 expression that were similar to those in the B95-8-infected cells (Fig. 4C). In the AdAH cells, NDRG1 was detected as a double band, and transfection of exogenous *NDRG1* cDNA produced a protein band that comigrated with the smaller band (data not shown). Both the larger and the smaller NDRG1 protein bands were downregulated in the BART(+)v-infected AdAH cells, and the downregulation disappeared in the revertant virus-infected cells (Fig. 4C).

These results indicate that downregulation of NDRG1 expression in the BART(+)v-infected cells occurs at both the mRNA and protein levels and that the 12-kb region of the EBV genome encompassing the BART miRNAs is responsible for the downregulation.

NDRG1 is expressed at a high level in epithelial cells but not B cells. It was previously reported that NDRG1 is expressed at a high level in epithelial cells (52); therefore, the expression levels of NDRG1 in various epithelium-derived cell lines were examined by immunoblotting. Substantial levels of NDRG1 expression were detected in AdAH cells, primary human bronchial epithelium-derived cells (HBEC1), human colon cancer-derived epithelial cell line Caco-2, human prostate cancer-derived epithelial cell line PC-3, and primary human prostate epithelium PrEC (Fig. 5). Consistent with the notion of its downregulation by EBV infec-

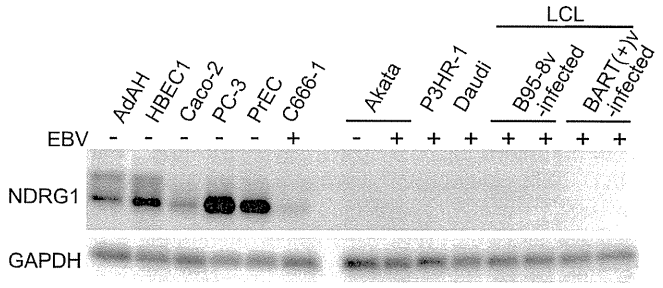

FIG 5 NDRG1 is expressed at a high level in epithelial cells but not B cells. Immunoblot analyses of NDRG1 and GAPDH protein levels in whole-cell extracts of various epithelial cells (AdAH cells, primary human bronchial epithelial HBEC1 cells, colon cancer-derived Caco-2 cells, prostate cancer-derived PC-3 cells, primary prostate epithelial PrEC cells [purchased from Lonza], and C666-1 cells) and B cells (Akata, P3HR-1, Daudi, and LCLs). The presence (+) or absence (−) of EBV infection in each cell line is indicated. The recombinant viruses used to establish the LCLs are indicated.

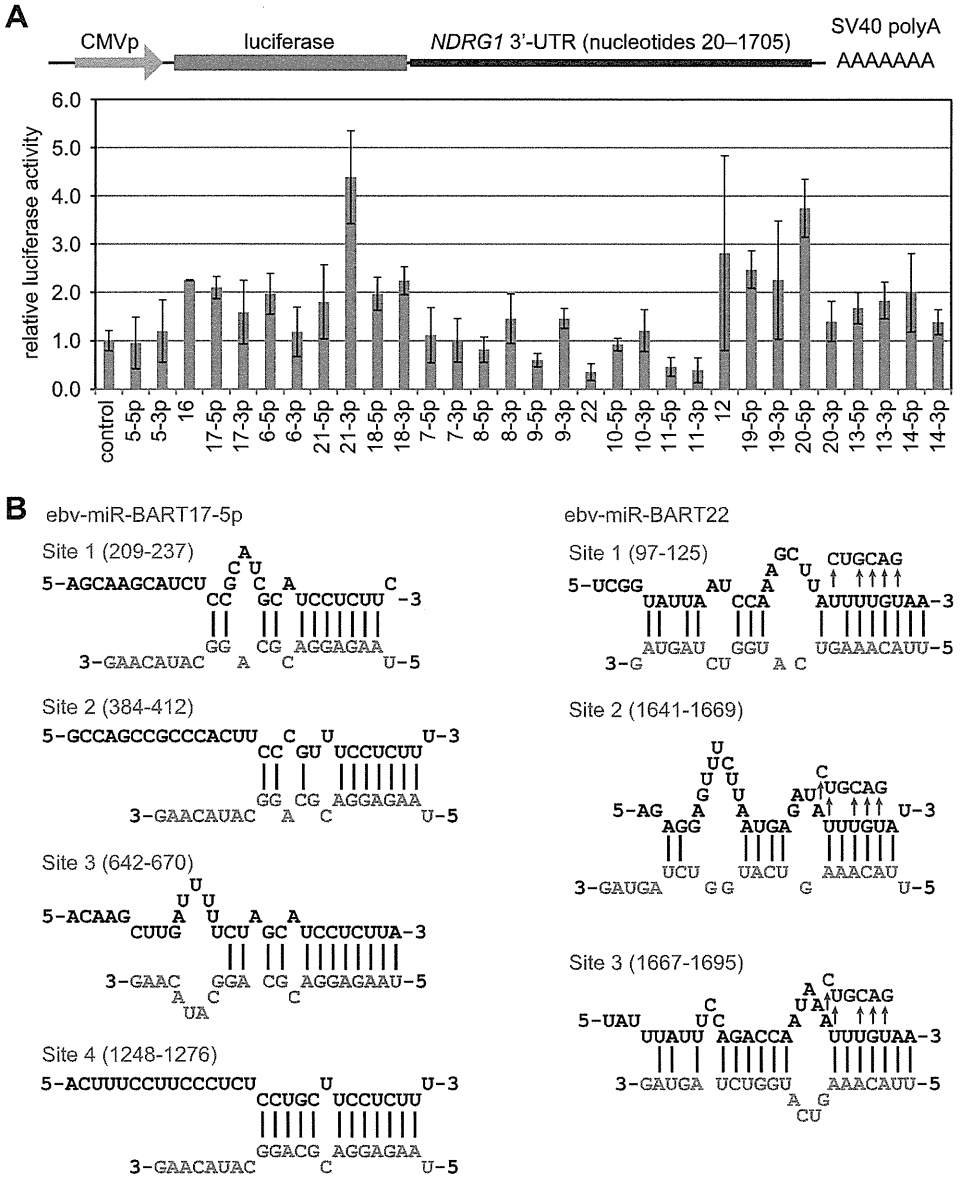

tion, the expression level of NDRG1 in C666-1 cells, which have abundant levels of BART miRNAs, was relatively low (Fig. 5). Although substantial levels of NDRG1 protein expression were detected in various epithelium-derived cells, Burkitt's lymphoma-derived cell lines (Akata, P3HR-1, and Daudi) and the LCLs barely expressed the NDRG1 protein (Fig. 5). These results indicate that, among EBV host cells, epithelial cells but not B cells express high levels of NDRG1 protein.

Screening of viral miRNAs putatively responsible for downregulating NDRG1 expression. Next, we investigated the possibility that BART miRNAs mediate the downregulation of NDRG1 expression directly in EBV-infected epithelial cells. Because miRNAs bind to specific sequences located within the 3′ UTR of a target mRNA (53), a reporter construct containing the 3′ UTR of *NDRG1* located between a luciferase open reading frame and a polyadenylation signal was constructed (Fig. 6A). The abilities of BART miRNA mimics corresponding to the 17 miRNAs encoded in the 12-kb deleted region of the EBV B95-8 strain (BART5, -16, -17, -6, -21, -18, -7, -8, -9, -22, -10, -11, -12, -19, -20, -13, and -14; indicated in gray in Fig. 1B) to downregulate luciferase gene expression in the B95-8v-infected HEK293 cells were determined. Some BART miRNA mimics upregulated the reporter, presumably due to their indirect effect on cytomegalovirus (CMV) promoter activity of the reporter gene. Thus, we focused on miRNA mimics that downregulated the reporter gene, The BART22 mimic suppressed the luciferase activity most strongly (Fig. 6A). This result agrees with that of a previous photoactivatable-ribonucleoside-enhanced cross-linking and immunoprecipitation analysis, which demonstrated that the *NDRG1* mRNA coprecipitates with BART17-5p and BART22 (32), both of which were expressed at high levels in the BART(+)v-infected HEK293 cells (Fig. 2A). BART9-5p, BART11-5p, and BART11-3p were also strong suppressors in the reporter assay (Fig. 6A). However, BART9-5p was hardly expressed in the infected cells (Fig. 2A), which had been demonstrated by deep sequencing (50, 54). BART11-5p and BART11-3p were found to suppress a reporter gene that lacked the NDRG1 3′ UTR (data not shown), suggesting they influence the expression of transcription factors that regulate CMV promoter of the reporter gene.

Although four putative BART17-5p binding sites and three putative BART22 were identified in the 3′ UTR of *NDRG1* using the miRNA target prediction program DIANA microT (51) (Fig. 6B), only the BART22 mimic downregulated the reporter gene expression (Fig. 6A and C). Notably, this mimic failed to downregulate luciferase gene expression when the three putative binding sites in the 3′ UTR of *NDRG1* were mutated (Fig. 6C). These results indicate that the downregulation of luciferase activity by the BART22 mimic was specifically dependent on the presence of the BART22 binding sites within the 3′ UTR of *NDRG1*. Transfection of B95.8v-infected HEK293 cells with the BART22 mimic also downregulated NDRG1 protein expression, while transfection of these cells with the BART17-5p mimic had no effect (Fig. 6D). This result supports the concept that BART22 is responsible for downregulating NDRG1 expression in EBV-infected epithelial cells.

Clustered EBV miRNAs cooperatively downregulate NDRG1 expression. The effects of BART miRNAs on NDRG1 expression were then verified by generating recombinant viruses containing specific deletions of BART miRNA genes. A BAC engineering technique was used to obtain modified EBV-BAC clones that specifically lacked the pre-miRNAs of BART22 only (BART22Δ), BART8 through BART11 (BART8-11Δ), or BART21 through BART14 (BART21-14Δ) (Fig. 7A). The genome of the BART21-14Δ virus, which had a 3.3-kb deletion, lacked the 13 pre-miRNA genes of cluster 2 BART miRNAs (18) but retained the three open reading frames (LF1, LF2, and LF3 in Fig. 1B). Restriction enzyme mapping of these BAC clone DNAs demonstrated that they did exhibit identical digestion pattern except for the fragments corresponding to the modified region (Fig. 7B, and see Table S7 in the supplemental material), and the result was verified by Southern blotting analyses using a specific probe for detecting the region (Fig. 7B). These modified BAC clones were stably transfected into HEK293 cells, and stably infected cell clones were established. Northern blot analyses demonstrated a specific loss of BART22 expression in the BART22Δv-infected cells (Fig. 7C). Immunoblot analyses indicated that NDRG1 was expressed at low levels in the BART22Δv-infected HEK293 cells, indicating that BART22 is not solely responsible for the downregulation of this protein (Fig. 7D). Similarly, NDRG1 was expressed at low levels in the BART8-11Δv-infected cells. However, NDRG1 expression levels were significantly higher in the BART21-14Δv-infected cells (Fig. 7D). No significant difference of viral latent gene expression was observed among the cells harboring different recombinant viruses; they expressed comparable levels of EBNA1, EBNA2, EBNA3s, and LMP1 (Fig. 7D). These results imply that clustered viral miRNAs cooperatively downregulate NDRG1 expression.

Metastatic prostate cancer-derived PC-3 cells, which expressed high levels of NDRG1 (Fig. 5), were then used as recipient cells of EBV infection to verify the results described above. PC-3 cells were transduced with CR2, infected with various recombinant EBVs, and pools of stably infected cells were established. Again, NDRG1 protein level was low in the BART(+)v-infected PC-3 cells, but the protein level recovered in the BART21-14Δv-infected cells (Fig. 7E). Only traces of EBNA1 protein, but no other viral latent

FIG 6 *NDRG1* is a target of the BART22 miRNA. (A) The upper panel shows a schematic illustration of the reporter construct containing the 3′ UTR of *NDRG1* between the luciferase gene (under the control of a cytomegalovirus immediate-early promoter, CMVp) and a simian virus 40 polyadenylation signal [poly(A)]. The lower panel shows the abilities of a series of BART miRNA mimics (indicated in gray in Fig. 1B) to downregulate luciferase activity in the B95.8v-infected HEK293 cells. The activity of firefly luciferase was normalized to that of *Renilla* luciferase (control), and the average values obtained by transfecting the control mimic were adjusted to 1. The data are represented as the means ± the SD of $n = 3$ independent experiments. (B) The predicted BART17-5p and BART22 target sequences in the 3′ UTR of *NDRG1*. The miRNA sequences are shown in green. The mutations introduced into the BART22 binding sites are indicated in blue. (C) BART17-5p mimic and BART22 mimic were tested for their abilities to downregulate the luciferase gene expression from the reporter construct shown in panel A or from a reporter construct containing mutations in the BART22 bindings sites in the *NDRG1* 3′ UTR. The B95.8v-infected HEK293 cells were used for the assay. The activity of firefly luciferase was normalized to that of *Renilla* luciferase (control), and the average values obtained by transfecting the control mimic were adjusted to 1. The data are represented as the means ± the SD of $n = 3$ independent experiments. (D) Immunoblot analyses of NDRG1 and GAPDH (control) protein levels in the B95.8v-infected HEK293 cells transfected with synthetic miRNA mimics (as indicated). The whole-cell extracts were prepared at 48 h posttransfection.

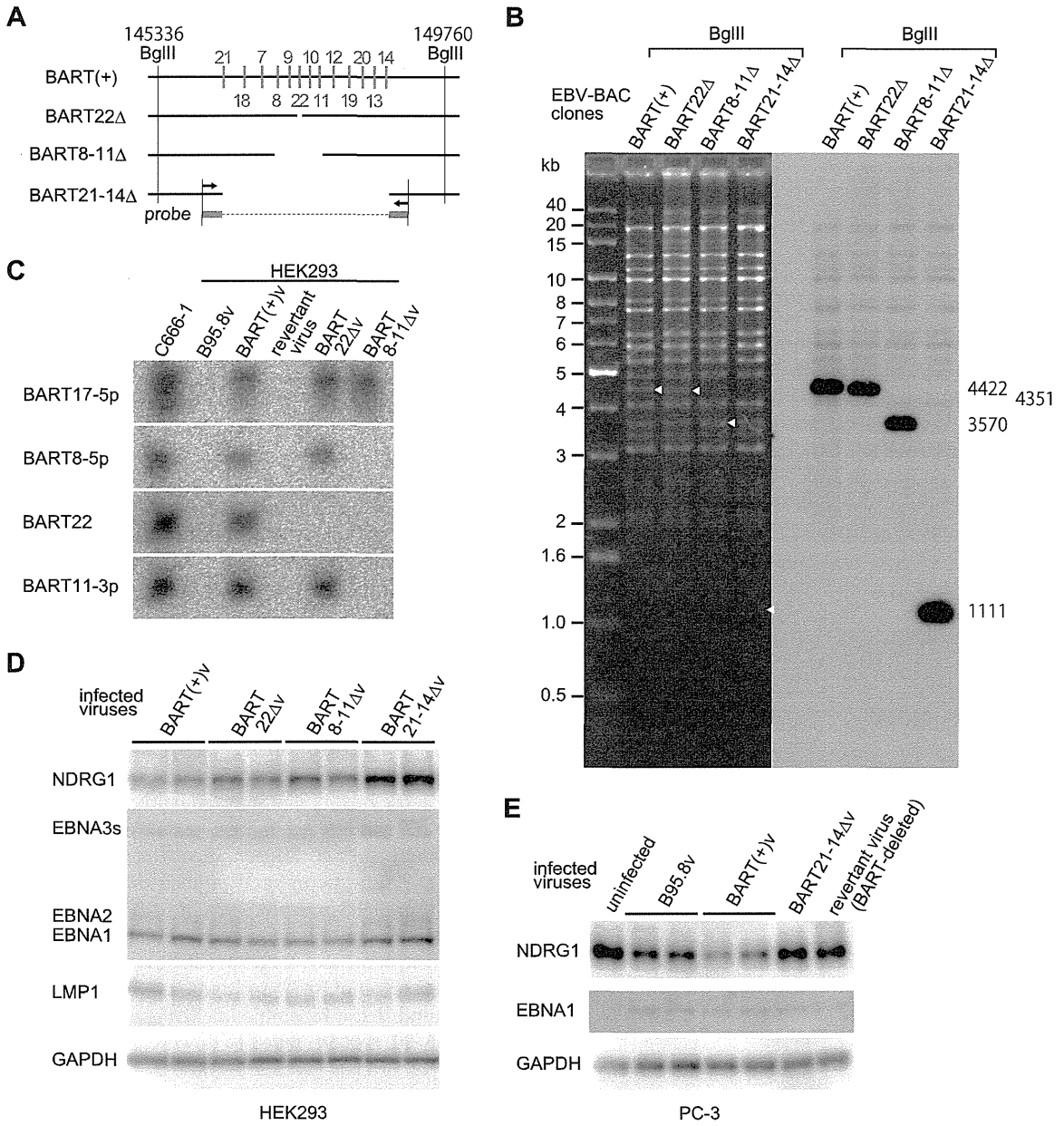

FIG 7 The EBV BART miRNA cluster 2 is responsible for the downregulation of NDRG1 expression. (A) Schematic illustrations of the BART miRNA cluster 2 deletion variants. The positions of the pre-miRNA genes are indicated by numbered vertical lines. The gaps in the horizontal lines indicate the deleted regions. The BglII sites flanking the region are indicated with nucleotide no. of EBV-wt. (B) The indicated EBV-BAC clone DNAs were digested with BglII and analyzed by agarose gel electrophoresis (left panel), and the gel was subsequently processed for Southern blot analysis (right panel). A DNA fragment of BART21-14Δ was PCR-amplified (arrows in panel A) and used as a probe. The bands representing the BART miRNA cluster 2 region (arrowheads in left) were detected by Southern blotting. The calculated sizes (see Table S7 in the supplemental material for the details) of the detected bands are indicated. (C) BART miRNA expression pattern of various recombinant viruses. Total RNAs of C666-1 cells and HEK293 cells infected with the indicated recombinant viruses were subjected to Northern blot analyses. Note that BART22Δ virus did not express BART22 miRNA but did express flanking miRNAs (BART8-5p and BART11-3p). (D) Protein levels of NDRG1, EBNAs, LMP1, and GAPDH in HEK293 cells infected with the indicated recombinant viruses (two independent cell clones for each virus). (E) Protein levels of NDRG1, EBNA1, and GAPDH in PC-3 cells infected with the indicated recombinant viruses.

proteins, were expressed in these cells (Fig. 7E and data not shown). The result reinforces the argument that the BART miRNA cluster 2 is responsible for the NDRG1 downregulation.

NDRG1 protein expression is downregulated in EBV-positive NPC tissues. The results thus far obtained indicate that NDRG1 was downregulated by BART miRNAs in EBV-infected epithelial cell cultures. We then examined whether NDRG1 was downregulated in EBV-positive epithelial tumors *in vivo*. The expression level of the NDRG1 protein in NPC biopsy specimens (Table 1) was examined by immunohistochemical staining. *In situ* hybridization (ISH) of EBV-encoded small RNA (EBER) was used to verify the presence of EBV infection. The results revealed that nine of the 10 EBER-ISH-negative NPC specimens were positive for NDRG1 expression (Table 1 and Fig. 8A). In contrast, six of the

TABLE 1 Clinicopathological features of the patients and the expression of NDRG1 in biopsy specimens

NPC type	No. of cases	Mean age (yr ± SD)[a]	No. of patients						
			WHO classification[b]			Stages[c]		NDRG1[d]	
			I	II	III	I, II	III, IV	–	+
EBER-ISH positive	9	54.0 ± 10.4	0	7	2	2	7	6	3
EBER-ISH negative	10	59.1 ± 8.0	1	8	1	3	7	1	9

[a] $P = 0.244$ (Student t test).
[b] $P = 0.509$ (χ^2 test).
[c] $P = 0.708$ (χ^2 test).
[d] $P = 0.02$ (Student t test).

nine EBER-ISH-positive NPC specimens were negative for NDRG1 expression (Table 1 and Fig. 8B). The difference between the NDRG1 expression levels in the EBER-ISH-positive and EBER-ISH-negative NPC specimens was statistically significant ($P = 0.02$; Table 1). These results indicate that downregulation of NDRG1 expression is common in EBER-ISH-positive NPC tissues and reinforce the biological significance of NDRG1 downregulation during NPC tumorigenesis.

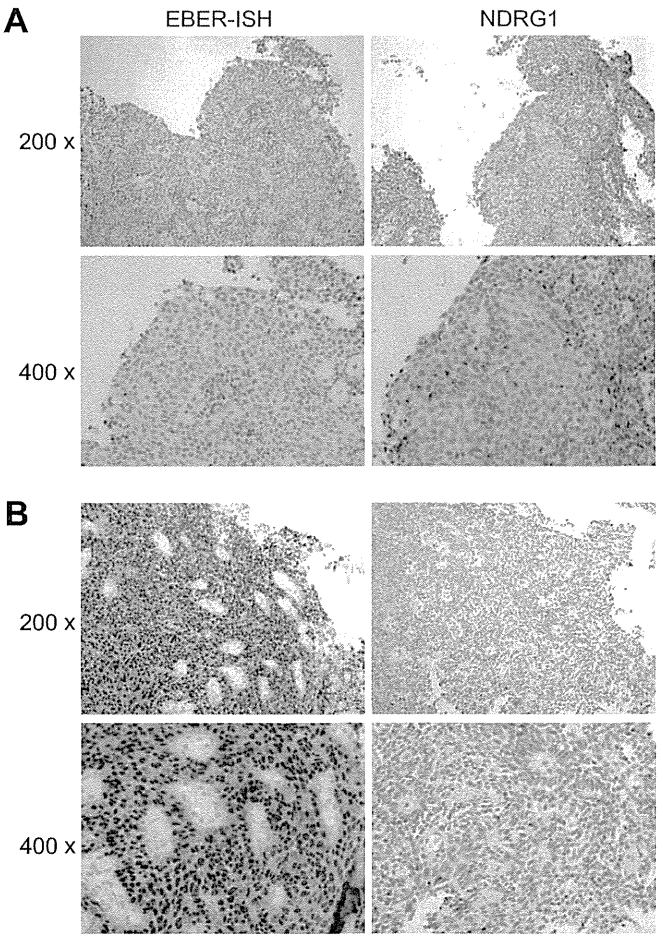

FIG 8 NDRG1 protein expression is downregulated in EBER-ISH-positive NPC biopsy specimens. (A and B) ISH analyses of EBER expression (left panels) and immunohistochemical analyses of NDRG1 expression (right panels) in NPC biopsy specimens. The magnifications are indicated. (A) Representative images of EBER-ISH-negative specimens. (B) Representative images of EBER-ISH-positive specimens.

DISCUSSION

It is well known that the commonly used EBV B95-8 strain lacks a 12-kb genomic region that is actively transcribed in EBV-positive epithelial malignancies. Recent studies have indicated that the transcripts encoded by this region are primary miRNAs that are processed to mature miRNAs (known as BART miRNAs). A few previous studies have successfully used recombinant EBV technology to investigate the roles of BART miRNAs (55, 56); however, to our knowledge, the specific roles of BART miRNAs in EBV-infected epithelial cells have not yet been analyzed using recombinant viruses.

Here, we established epithelial cells that were latently infected with the EBV B95-8 virus lacking the actively transcribed 12-kb region, or the BART(+) virus in which this region was restored using BAC technology. The 12-kb region encodes 17 of the 22 BART miRNAs and three open reading frames (LF1, LF2, and LF3). Physiological levels of BART miRNA expression were reconstituted in the BART(+)v-infected epithelial cells. In our system, the BART miRNA genes were seamlessly restored at their native loci and expressed under the control of their native promoters (57). This experimental strategy likely contributes to achieve appropriate expression levels of BART miRNAs.

Via unbiased screening under physiological conditions, in combination with miRNA target prediction, NDRG1 was identified as a direct target of BART miRNAs in EBV-infected epithelial cells. We found that a recombinant EBV lacking BART miRNA cluster 2 (BART21-14Δv) failed to downregulate NDRG1 in two different types of cells (HEK293 and PC-3 cells). Since BART miRNA cluster 2 is located within the intron of BART mRNA, open reading frames of putative BART-encoded protein(s) are preserved in the BART21-14Δ recombinant virus. Furthermore, the BART21-14Δ virus retains intact LF1, LF2, and LF3 open reading frames as well. Therefore, although we cannot completely exclude the possibility that altered expression of putative viral protein(s) encoded by BART mRNA somehow contribute to this NDRG1 dysregulation, it is highly likely that BART miRNAs *per se* are responsible for the NDRG1 downregulation. Transfection assay using BART miRNA mimics identified the BART22 miRNA mimic as the strongest suppressor of NDRG1 expression at both mRNA and protein levels. This is in good agreement with the previous report that NDRG1 mRNA was in complex with BART17-5p and BART22 in primary effusion lymphoma cell lines (32). It is important to note that BART22 is one of the highly expressed BART miRNAs in EBV-infected epithelial cells (9, 54, 58). However, a recombinant EBV lacking the BART22 pre-miRNA gene (BART22Δv) was still able to downregulate NDRG1 expression. This apparent inconsistency can be interpreted that

miRNA-mediated gene regulation is highly redundant; other viral miRNAs likely can compensate for the loss of BART22. BART miRNAs may also bind to 5′ UTR and/or the coding region of NDRG1 mRNA to downregulate protein expression. BART miRNA-mediated downregulation of NDRG1 may not be restricted to direct interaction between BART miRNAs and NDRG1 mRNA. Furthermore, the use of miRNA target prediction programs revealed that NDRG1 may be targeted by several cellular miRNAs, including miR-182, a well-known metastasis-regulatory miRNA (59). Further investigations of the cooperative effects of viral and cellular miRNAs are warranted.

NDRG1 expression increases in response to cell differentiation signals (52, 60). Our results indicate that NDRG1 is expressed at high levels in primary epithelial cells (Fig. 5). Therefore, a possible scenario is that when EBV infects cells in epithelial lineages *in vivo*, BART miRNA targets NDRG1 to avoid growth arrest and terminal differentiation. Alternatively, EBV may preferentially establish latent infection in undifferentiated epithelial cells with little NDRG1 expression, assuming that NDRG1 expression is disadvantageous for the proliferation of the infected cells. NDRG1 has also been characterized as a metastasis suppressor (61), although its antimetastatic potential was mostly demonstrated by overexpressing NDRG1 in tumor cells. Due to its pleiotropic functions of NDRG1 protein (60), it is currently difficult to envision how NDRG1 downregulation contributes to epithelial carcinogenesis. A recent study indicated that NDRG1 interacts with the Wnt receptor LRP6 and blocks Wnt signaling (62). Thus, NDRG1 downregulation may contribute to the activation of Wnt signaling pathway, which is common in gastrointestinal epithelium-derived malignancies (63). For note, other regulators of Wnt signaling pathway, such as CARPIN2 (24) and DAZAP2 (27), were also identified as BART miRNA targets (64).

For unknown reasons, most of the previously identified BART miRNA targets were not identified under the experimental conditions used here; NDRG1 (32) and API5 (30) are the two exceptions (See Dataset S1 and Table S5 in the supplemental material). API5 protein levels were also examined in the established cells, but downregulation of API5 in the BART(+)v-infected cells was not as apparent as that of NDRG1 at the protein level (data not shown).

Thus far, we have found no obvious phenotypic differences between the B95.8v-infected and BART(+)v-infected epithelial cells in their morphologies and proliferation rates. This can be interpreted that one should instead use primary epithelial cells as recipient cells. Alternatively, it may be that BART miRNAs should cooperate with viral oncoproteins to induce phenotypic changes in infected epithelial cells. Importantly, it is known that the viral major oncoprotein LMP1 encoded by NPC-derived EBV is functionally different from that encoded by the B95-8 strain EBV (65); therefore, it may be critical to examine the roles of BART miRNAs in the presence of NPC-derived LMP1 protein. The EBV-BAC technology described in the present study should be useful for further clarifying the mechanism of EBV-mediated epithelial carcinogenesis.

ACKNOWLEDGMENTS

This study was supported by JSPS Kakenhi grant 24590567, by a Grant-in-Aid for Scientific Research from the Ministry of Health, Labor, and Welfare, Japan, by the Uehara Memorial Foundation, and by the Takeda Science Foundation.

REFERENCES

1. **Rickinson AB, Kieff E.** 2007. Epstein-Barr virus, p 2603–2654. *In* Knipe DM, Howley PM (ed), Fields virology, 5th ed. Lippincott/The Williams & Wilkins Co, Philadelphia, PA.
2. **Miller G, Lipman M.** 1973. Release of infectious Epstein-Barr virus by transformed marmoset leukocytes. Proc Natl Acad Sci U S A **70**:190–194. http://dx.doi.org/10.1073/pnas.70.1.190.
3. **Baer R, Bankier AT, Biggin MD, Deininger PL, Farrell PJ, Gibson TJ, Hatfull G, Hudson GS, Satchwell SC, Seguin C.** 1984. DNA sequence and expression of the B95-8 Epstein-Barr virus genome. Nature **310**:207–211. http://dx.doi.org/10.1038/310207a0.
4. **Raab-Traub N, Dambaugh T, Kieff E.** 1980. DNA of Epstein-Barr virus VIII: B95-8, the previous prototype, is an unusual deletion derivative. Cell **22**:257–267. http://dx.doi.org/10.1016/0092-8674(80)90173-7.
5. **Skare J, Edson C, Farley J, Strominger JL.** 1982. The B95-8 isolate of Epstein-Barr virus arose from an isolate with a standard genome. J Virol **44**:1088–1091.
6. **Cai X, Schafer A, Lu S, Bilello JP, Desrosiers RC, Edwards R, Raab-Traub N, Cullen BR.** 2006. Epstein-Barr virus microRNAs are evolutionarily conserved and differentially expressed. PLoS Pathog **2**:e23. http://dx.doi.org/10.1371/journal.ppat.0020023.
7. **Grundhoff A, Sullivan CS, Ganem D.** 2006. A combined computational and microarray-based approach identifies novel microRNAs encoded by human gammaherpesviruses. RNA **12**:733–750. http://dx.doi.org/10.1261/rna.2326106.
8. **Pfeffer S, Zavolan M, Grasser FA, Chien M, Russo JJ, Ju J, John B, Enright AJ, Marks D, Sander C, Tuschl T.** 2004. Identification of virus-encoded microRNAs. Science **304**:734–736. http://dx.doi.org/10.1126/science.1096781.
9. **Zhu JY, Pfuhl T, Motsch N, Barth S, Nicholls J, Grasser F, Meister G.** 2009. Identification of novel Epstein-Barr virus microRNA genes from nasopharyngeal carcinomas. J Virol **83**:3333–3341. http://dx.doi.org/10.1128/JVI.01689-08.
10. **Hitt MM, Allday MJ, Hara T, Karran L, Jones MD, Busson P, Tursz T, Ernberg I, Griffin BE.** 1989. EBV gene expression in an NPC-related tumour. EMBO J **8**:2639–2651.
11. **Gilligan KJ, Rajadurai P, Lin JC, Busson P, Abdel-Hamid M, Prasad U, Tursz T, Raab-Traub N.** 1991. Expression of the Epstein-Barr virus BamHI A fragment in nasopharyngeal carcinoma: evidence for a viral protein expressed in vivo. J Virol **65**:6252–6259.
12. **Sadler RH, Raab-Traub N.** 1995. Structural analyses of the Epstein-Barr virus BamHI A transcripts. J Virol **69**:1132–1141.
13. **Smith PR, de Jesus O, Turner D, Hollyoake M, Karstegl CE, Griffin BE, Karran L, Wang Y, Hayward SD, Farrell PJ.** 2000. Structure and coding content of CST (BART) family RNAs of Epstein-Barr virus. J Virol **74**:3082–3092. http://dx.doi.org/10.1128/JVI.74.7.3082-3092.2000.
14. **Edwards RH, Marquitz AR, Raab-Traub N.** 2008. Epstein-Barr virus BART microRNAs are produced from a large intron prior to splicing. J Virol **82**:9094–9106. http://dx.doi.org/10.1128/JVI.00785-08.
15. **Cosmopoulos K, Pegtel M, Hawkins J, Moffett H, Novina C, Middeldorp J, Thorley-Lawson DA.** 2009. Comprehensive profiling of Epstein-Barr virus microRNAs in nasopharyngeal carcinoma. J Virol **83**:2357–2367. http://dx.doi.org/10.1128/JVI.02104-08.
16. **Kim do N, Chae HS, Oh ST, Kang JH, Park CH, Park WS, Takada K, Lee JM, Lee WK, Lee SK.** 2007. Expression of viral microRNAs in Epstein-Barr virus-associated gastric carcinoma. J Virol **81**:1033–1036. http://dx.doi.org/10.1128/JVI.02271-06.
17. **Ramakrishnan R, Donahue H, Garcia D, Tan J, Shimizu N, Rice AP, Ling PD.** 2011. Epstein-Barr virus BART9 miRNA modulates LMP1 levels and affects growth rate of nasal NK T cell lymphomas. PLoS One **6**:e27271. http://dx.doi.org/10.1371/journal.pone.0027271.
18. **Lo AK, Dawson CW, Jin DY, Lo KW.** 2012. The pathological roles of BART miRNAs in nasopharyngeal carcinoma. J Pathol **227**:392–403. http://dx.doi.org/10.1002/path.4025.
19. **Marquitz AR, Raab-Traub N.** 2012. The role of miRNAs and EBV BARTs in NPC. Semin Cancer Biol **22**:166–172. http://dx.doi.org/10.1016/j.semcancer.2011.12.001.
20. **Raab-Traub N.** 2012. Novel mechanisms of EBV-induced oncogenesis. Curr Opin Virol **2**:453–458. http://dx.doi.org/10.1016/j.coviro.2012.07.001.
21. **Barth S, Pfuhl T, Mamiani A, Ehses C, Roemer K, Kremmer E, Jaker C, Hock J, Meister G, Grasser FA.** 2008. Epstein-Barr virus-encoded

microRNA miR-BART2 downregulates the viral DNA polymerase BALF5. Nucleic Acids Res 36:666–675.
22. Lo AK, To KF, Lo KW, Lung RW, Hui JW, Liao G, Hayward SD. 2007. Modulation of LMP1 protein expression by EBV-encoded microRNAs. Proc Natl Acad Sci U S A 104:16164–16169. http://dx.doi.org/10.1073/pnas.0702896104.
23. Lung RW, Tong JH, Sung YM, Leung PS, Ng DC, Chau SL, Chan AW, Ng EK, Lo KW, To KF. 2009. Modulation of LMP2A expression by a newly identified Epstein-Barr virus-encoded microRNA miR-BART22. Neoplasia 11:1174–1184.
24. Riley KJ, Rabinowitz GS, Yario TA, Luna JM, Darnell RB, Steitz JA. 2012. EBV and human microRNAs co-target oncogenic and apoptotic viral and human genes during latency. EMBO J 31:2207–2221. http://dx.doi.org/10.1038/emboj.2012.63.
25. Marquitz AR, Mathur A, Nam CS, Raab-Traub N. 2011. The Epstein-Barr Virus BART microRNAs target the proapoptotic protein Bim. Virology 412:392–400. http://dx.doi.org/10.1016/j.virol.2011.01.028.
26. Vereide DT, Seto E, Chiu YF, Hayes M, Tagawa T, Grundhoff A, Hammerschmidt W, Sugden B. 2014. Epstein-Barr virus maintains lymphomas via its miRNAs. Oncogene 33:1258–1264. http://dx.doi.org/10.1038/onc.2013.71.
27. Skalsky RL, Corcoran DL, Gottwein E, Frank CL, Kang D, Hafner M, Nusbaum JD, Feederle R, Delecluse HJ, Luftig MA, Tuschl T, Ohler U, Cullen BR. 2012. The viral and cellular microRNA targetome in lymphoblastoid cell lines. PLoS Pathog 8:e1002484. http://dx.doi.org/10.1371/journal.ppat.1002484.
28. Iizasa H, Wulff BE, Alla NR, Maragkakis M, Megraw M, Hatzigeorgiou A, Iwakiri D, Takada K, Wiedmer A, Showe L, Lieberman P, Nishikura K. 2010. Editing of Epstein-Barr virus-encoded BART6 microRNAs controls their dicer targeting and consequently affects viral latency. J Biol Chem 285:33358–33370. http://dx.doi.org/10.1074/jbc.M110.138362.
29. Hsu CY, Yi YH, Chang KP, Chang YS, Chen SJ, Chen HC. 2014. The Epstein-Barr virus-encoded microRNA MiR-BART9 promotes tumor metastasis by targeting E-cadherin in nasopharyngeal carcinoma. PLoS Pathog 10:e1003974. http://dx.doi.org/10.1371/journal.ppat.1003974.
30. Dolken L, Malterer G, Erhard F, Kothe S, Friedel CC, Suffert G, Marcinowski L, Motsch N, Barth S, Beitzinger M, Lieber D, Bailer SM, Hoffmann R, Ruzsics Z, Kremmer E, Pfeffer S, Zimmer R, Koszinowski UH, Grasser F, Meister G, Haas J. 2010. Systematic analysis of viral and cellular microRNA targets in cells latently infected with human gammaherpesviruses by RISC immunoprecipitation assay. Cell Host Microbe 7:324–334. http://dx.doi.org/10.1016/j.chom.2010.03.008.
31. Choy EY, Siu KL, Kok KH, Lung RW, Tsang CM, To KF, Kwong DL, Tsao SW, Jin DY. 2008. An Epstein-Barr virus-encoded microRNA targets PUMA to promote host cell survival. J Exp Med 205:2551–2560. http://dx.doi.org/10.1084/jem.20072581.
32. Gottwein E, Corcoran DL, Mukherjee N, Skalsky RL, Hafner M, Nusbaum JD, Shamulailatpam P, Love CL, Dave SS, Tuschl T, Ohler U, Cullen BR. 2011. Viral microRNA targetome of KSHV-infected primary effusion lymphoma cell lines. Cell Host Microbe 10:515–526. http://dx.doi.org/10.1016/j.chom.2011.09.012.
33. Feederle R, Bartlett EJ, Delecluse HJ. 2010. Epstein-Barr virus genetics: talking about the BAC generation. Herpesviridae 1:6. http://dx.doi.org/10.1186/2042-4280-1-6.
34. Shaw G, Morse S, Ararat M, Graham FL. 2002. Preferential transformation of human neuronal cells by human adenoviruses and the origin of HEK 293 cells. FASEB J 16:869–871. http://dx.doi.org/10.1096/fj.01-0995fje.
35. Delecluse HJ, Hilsendegen T, Pich D, Zeidler R, Hammerschmidt W. 1998. Propagation and recovery of intact, infectious Epstein-Barr virus from prokaryotic to human cells. Proc Natl Acad Sci U S A 95:8245–8250. http://dx.doi.org/10.1073/pnas.95.14.8245.
36. Takada K, Horinouchi K, Ono Y, Aya T, Osato T, Takahashi M, Hayasaka S. 1991. An Epstein-Barr virus-producer line Akata: establishment of the cell line and analysis of viral DNA. Virus Genes 5:147–156. http://dx.doi.org/10.1007/BF00571929.
37. Strong MJ, Baddoo M, Nanbo A, Xu M, Puetter A, Lin Z. 2014. Comprehensive RNA-seq analysis reveals contamination of multiple nasopharyngeal carcinoma cell lines with HeLa cell genomes. J Virol 88:10696–10704. http://dx.doi.org/10.1128/JVI.01457-14.
38. Takimoto T, Sato H, Ogura H, Miyawaki T, Glaser R. 1986. Superinfection of epithelial hybrid cells (D98/HR-1, NPC-KT, and A2L/AH) with Epstein-Barr virus and the relationship to the C3d receptor. Cancer Res 46:2541–2544.
39. Cheung ST, Huang DP, Hui AB, Lo KW, Ko CW, Tsang YS, Wong N, Whitney BM, Lee JC. 1999. Nasopharyngeal carcinoma cell line (C666-1) consistently harbouring Epstein-Barr virus. Int J Cancer 83:121–126. http://dx.doi.org/10.1002/(SICI)1097-0215(19990924)83:1<121::AID-IJC21>3.0.CO;2-F.
40. Kanda T, Shibata S, Saito S, Murata T, Isomura H, Yoshiyama H, Takada K, Tsurumi T. 2011. Unexpected instability of family of repeats (FR), the critical *cis*-acting sequence required for EBV latent infection, in EBV-BAC systems. PLoS One 6:e27758. http://dx.doi.org/10.1371/journal.pone.0027758.
41. Kanda T, Yajima M, Ahsan N, Tanaka M, Takada K. 2004. Production of high-titer Epstein-Barr virus recombinants derived from Akata cells by using a bacterial artificial chromosome system. J Virol 78:7004–7015. http://dx.doi.org/10.1128/JVI.78.13.7004-7015.2004.
42. Nakano Y, Yoshida Y, Yamashita Y, Koga T. 1995. Construction of a series of pACYC-derived plasmid vectors. Gene 162:157–158. http://dx.doi.org/10.1016/0378-1119(95)00320-6.
43. Fruscalzo A, Marsili G, Busiello V, Bertolini L, Frezza D. 2001. DNA sequence heterogeneity within the Epstein-Barr virus family of repeats in the latent origin of replication. Gene 265:165–173. http://dx.doi.org/10.1016/S0378-1119(01)00345-6.
44. Kanda T, Horikoshi N, Murata T, Kawashima D, Sugimoto A, Narita Y, Kurumizaka H, Tsurumi T. 2013. Interaction between basic residues of Epstein-Barr virus EBNA1 protein and cellular chromatin mediates viral plasmid maintenance. J Biol Chem 288:24189–24199. http://dx.doi.org/10.1074/jbc.M113.491167.
45. Chen C, Ridzon DA, Broomer AJ, Zhou Z, Lee DH, Nguyen JT, Barbisin M, Xu NL, Mahuvakar VR, Andersen MR, Lao KQ, Livak KJ, Guegler KJ. 2005. Real-time quantification of microRNAs by stem-loop RT-PCR. Nucleic Acids Res 33:e179. http://dx.doi.org/10.1093/nar/gni178.
46. Shimada A, Dohke K, Sadaie M, Shinmyozu K, Nakayama J, Urano T, Murakami Y. 2009. Phosphorylation of Swi6/HP1 regulates transcriptional gene silencing at heterochromatin. Genes Dev 23:18–23. http://dx.doi.org/10.1101/gad.1708009.
47. Kitagawa N, Kondo S, Wakisaka N, Zen Y, Nakanishi Y, Tsuji A, Endo K, Murono S, Yoshizaki T. 2013. Expression of seven-in-absentia homologue 1 and hypoxia-inducible factor 1 alpha: novel prognostic factors of nasopharyngeal carcinoma. Cancer Lett 331:52–57. http://dx.doi.org/10.1016/j.canlet.2012.12.002.
48. de Jesus O, Smith PR, Spender LC, Elgueta Karstegl C, Niller HH, Huang D, Farrell PJ. 2003. Updated Epstein-Barr virus (EBV) DNA sequence and analysis of a promoter for the BART (CST, BARF0) RNAs of EBV. J Gen Virol 84:1443–1450. http://dx.doi.org/10.1099/vir.0.19054-0.
49. Bloss TA, Sugden B. 1994. Optimal lengths for DNAs encapsidated by Epstein-Barr virus. J Virol 68:8217–8222.
50. Qiu J, Cosmopoulos K, Pegtel M, Hopmans E, Murray P, Middeldorp J, Shapiro M, Thorley-Lawson DA. 2011. A novel persistence associated EBV miRNA expression profile is disrupted in neoplasia. PLoS Pathog 7:e1002193. http://dx.doi.org/10.1371/journal.ppat.1002193.
51. Paraskevopoulou MD, Georgakilas G, Kostoulas N, Vlachos IS, Vergoulis T, Reczko M, Filippidis C, Dalamagas T, Hatzigeorgiou AG. 2013. DIANA-microT web server v5.0: service integration into miRNA functional analysis workflows. Nucleic Acids Res 41:W169–W173. http://dx.doi.org/10.1093/nar/gkt393.
52. Lachat P, Shaw P, Gebhard S, van Belzen N, Chaubert P, Bosman FT. 2002. Expression of NDRG1, a differentiation-related gene, in human tissues. Histochem Cell Biol 118:399–408. http://dx.doi.org/10.1007/s00418-002-0460-9.
53. Bartel DP. 2009. MicroRNAs: target recognition and regulatory functions. Cell 136:215–233. http://dx.doi.org/10.1016/j.cell.2009.01.002.
54. Marquitz AR, Mathur A, Chugh PE, Dittmer DP, Raab-Traub N. 2014. Expression Profile of MicroRNAs in Epstein-Barr Virus-Infected AGS Gastric Carcinoma Cells. J Virol 88:1389–1393. http://dx.doi.org/10.1128/JVI.02662-13.
55. Klinke O, Feederle R, Delecluse HJ. 2014. Genetics of Epstein-Barr virus microRNAs. Semin Cancer Biol 26:52–59. http://dx.doi.org/10.1016/j.semcancer.2014.02.002.
56. Seto E, Moosmann A, Gromminger S, Walz N, Grundhoff A, Hammerschmidt W. 2010. Micro RNAs of Epstein-Barr virus promote cell cycle progression and prevent apoptosis of primary human B cells. PLoS Pathog 6:e1001063. http://dx.doi.org/10.1371/journal.ppat.1001063.
57. Chen H, Huang J, Wu FY, Liao G, Hutt-Fletcher L, Hayward SD. 2005. Regulation of expression of the Epstein-Barr virus BamHI-A rightward

transcripts. J Virol **79:**1724–1733. http://dx.doi.org/10.1128/JVI.79.3.1724-1733.2005.

58. **Walz N, Christalla T, Tessmer U, Grundhoff A.** 2010. A global analysis of evolutionary conservation among known and predicted gammaherpesvirus microRNAs. J Virol **84:**716–728. http://dx.doi.org/10.1128/JVI.01302-09.
59. **Hurst DR, Edmonds MD, Welch DR.** 2009. Metastamir: the field of metastasis-regulatory microRNA is spreading. Cancer Res **69:**7495–7498. http://dx.doi.org/10.1158/0008-5472.CAN-09-2111.
60. **Ellen TP, Ke Q, Zhang P, Costa M.** 2008. NDRG1, a growth and cancer related gene: regulation of gene expression and function in normal and disease states. Carcinogenesis **29:**2–8.
61. **Kovacevic Z, Richardson DR.** 2006. The metastasis suppressor, Ndrg-1: a new ally in the fight against cancer. Carcinogenesis **27:**2355–2366. http://dx.doi.org/10.1093/carcin/bgl146.
62. **Liu W, Xing F, Iiizumi-Gairani M, Okuda H, Watabe M, Pai SK, Pandey PR, Hirota S, Kobayashi A, Mo YY, Fukuda K, Li Y, Watabe K.** 2012. N-myc downstream regulated gene 1 modulates Wnt-beta-catenin signaling and pleiotropically suppresses metastasis. EMBO Mol Med **4:**93–108. http://dx.doi.org/10.1002/emmm.201100190.
63. **White BD, Chien AJ, Dawson DW.** 2012. Dysregulation of Wnt/beta-catenin signaling in gastrointestinal cancers. Gastroenterology **142:**219–232. http://dx.doi.org/10.1053/j.gastro.2011.12.001.
64. **Kuzembayeva M, Hayes M, Sugden B.** 2014. Multiple functions are mediated by the miRNAs of Epstein-Barr virus. Curr Opin Virol **7:**61–65. http://dx.doi.org/10.1016/j.coviro.2014.04.003.
65. **Dawson CW, Eliopoulos AG, Blake SM, Barker R, Young LS.** 2000. Identification of functional differences between prototype Epstein-Barr virus-encoded LMP1 and a nasopharyngeal carcinoma-derived LMP1 in human epithelial cells. Virology **272:**204–217. http://dx.doi.org/10.1006/viro.2000.0344.

Twin studies on the effect of genetic factors on serum agalactosyl immunoglobulin G levels

KANAKO AZUMA[1*], SHINICHIRO SHINZAKI[1*], HITOMI ASAZAWA[1*], ERI KUROKI[1], SAYURI KAWAMOTO[1], YOSHIHIRO KAMADA[1], KAZUO HAYAKAWA[2] and EIJI MIYOSHI[1]

Departments of [1]Molecular Biochemistry and Clinical Investigation and [2]Health Promotion Science, Osaka University Graduate School of Medicine, Suita, Osaka 565-0871, Japan

Received November 5, 2013; Accepted December 20, 2013

DOI: 10.3892/br.2014.216

Abstract. The level of immunoglobulin G (IgG) lacking the terminal galactose, referred to as agalactosyl IgG, was found to be increased in chronic inflammatory diseases, such as rheumatoid arthritis and inflammatory bowel disease (IBD), particularly in Crohn's disease, which is suggested to have a genetic component. This oligosaccharide modification of IgG is mainly regulated by the expression of glyco-genes; however, the association between genetic factors and changes in the IgG glycosylation has not been fully elucidated. The aim of the present study was to assess the role of genetics in this process by comparing the serum agalactosyl IgG levels between members of monozygotic and dizygotic twin pairs who underwent medical check-ups at the same time. The serum agalactosyl IgG level was assayed using high-performance liquid chromatography. Hematological and biochemical markers, including γ-glutamyltranspeptidase (γGTP), alanine aminotransferase (ALT) and white blood cell (WBC) count, were also measured. Although the serum γGTP levels (and, to a lesser extent, ALT and WBC levels) exhibited a correlation within monozygotic twin pairs, agalactosyl IgG levels were not found to be correlated between members of either type of twin pairs. Thus, the role of genetic factors in determining serum agalactosyl IgG levels may be less significant compared to the effect of environmental factors or the onset of inflammatory disease.

Correspondence to: Professor Eiji Miyoshi, Department of Molecular Biochemistry and Clinical Investigation, Osaka University Graduate School of Medicine, 1-7 Yamada-oka, Suita 565-0871, Osaka, Japan
E-mail: emiyoshi@sahs.med.osaka-u.ac.jp

*Contributed equally

Abbreviations: IgG, immunoglobulin G; IBD, inflammatory bowel disease

Key words: agalactosyl immunoglobulin G, environmental factors, genetic factors, monozygotic twin pairs, dizygotic twin pairs

Introduction

Immunoglobulin G (IgG) possesses complex-type biantennary *N*-linked oligosaccharides at asparagine 297 of the Cγ2 domain of the Fc fragment (1). Some of these oligosaccharides have bisecting *N*-acetylglucosamine (GlcNAc), core-fucose, galactose and sialic acid residues (2,3). Patients with rheumatoid arthritis (4) and other chronic inflammatory diseases, such as systemic lupus erythematosus, Sjogren's syndrome and tuberculosis (5,6), exhibit elevated serum levels of agalactosyl IgG, an IgG oligosaccharide that lacks the terminal galactose. We recently reported that serum agalactosyl IgG levels may be a novel diagnostic marker for the activity and clinical course of inflammatory bowel disease (IBD) (7) and developed a method to determine agalactosyl IgG using a lectin-antibody ELISA (8). Furthermore, we demonstrated the pathophysiological role of agalactosyl IgG in IBD using a mouse model of experimental colitis that is deficient in β-1,4-galactosyltransferase (9). Those experiments indicated that the increase in agalactosyl IgG levels in patients with IBD may be associated with the host's defense against inflammation, rather than the etiology of IBD.

We previously evaluated the levels of agalactosyl IgG by measuring the ratio of agalactosylated to fucosylated IgG oligosaccharides (G0F/G2F) (7) and demonstrated that G0F/G2F is a marker of IBD clinical activity and prognosis of recurrence. However, some patients with Crohn's disease do not exhibit elevated agalactosyl IgG levels, despite severe disease activity, suggesting that genetic factors may dictate IgG galactosylation. Furthermore, the level of IgG agalactosylation was shown to increase with age (10) and may be regulated by a variety of environmental factors, including food and infection; therefore, the relative effect of genetic and environmental factors has not been clearly determined. To determine the effect of genetic factors on the agalactosylation of IgG, we investigated the correlations of G0F/G2F and other biochemical data within pairs of monozygotic and dizygotic twins who underwent simultaneous medical check-ups.

Materials and methods

Subjects. The characteristics of the participants are summarized in Table I. Sixteen monozygotic twin pairs (14 males and 18 females, aged 40.8±19.3 years) and 13 dizygotic twin pairs

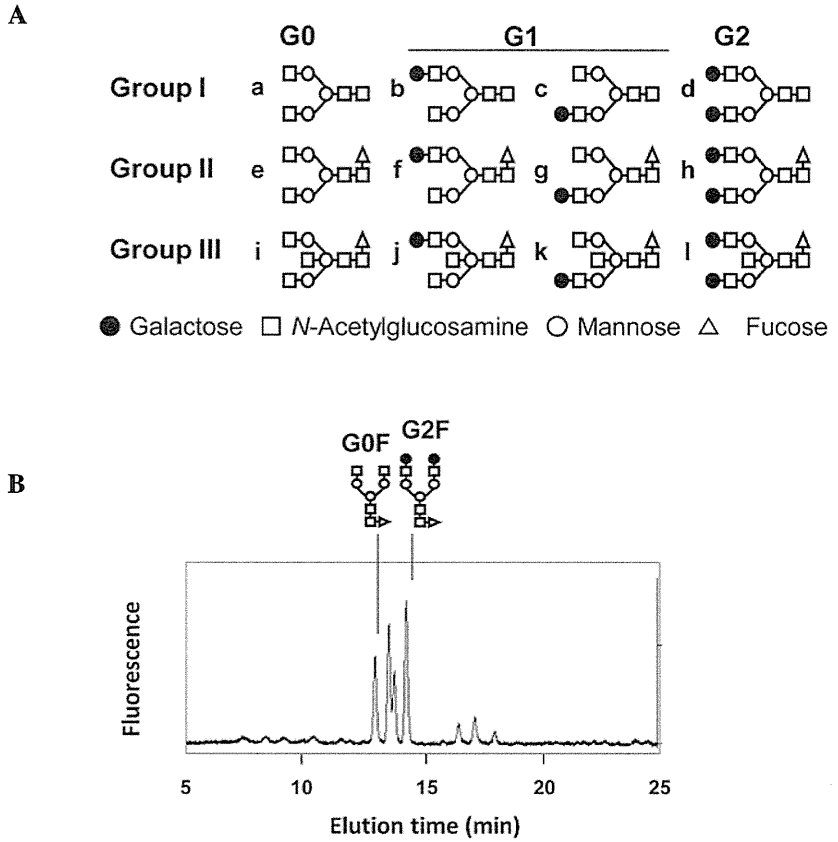

Figure 1. Analysis of 2pyridylamino (PA)-labeled IgG oligosaccharides with high-performance liquid chromatography. (A) Structural patterns of N-linked neutral oligosaccharides on IgG. (B) Representative profiles of 2PA-labeled oligosaccharides derived from IgG under neutral conditions.

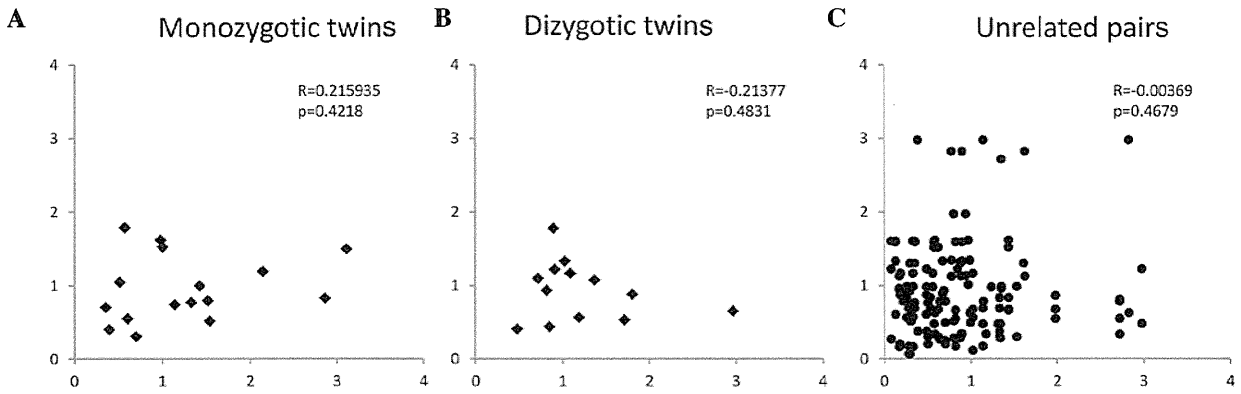

Figure 2. Scatterplots of G0F/G2F ratios for (A) monozygotic twins; (B) dizygotic twins; and (C) unrelated pairs. In (A) and (B), the higher G0F/G2F ratio within the pair was plotted on the horizontal axis.

Table I. Subject participant characteristics (means ± SD).

Characteristics	Monozygotic twins	Dizygotic twins
Pairs (n)	16	13
Male/female	14/18	10/16
Age (years)	40.8±19.3	42.5±16.9
γ-glutamyltranspeptidase (IU/l)	25.4±25.7	22.8±35.4
Alanine aminotransferase (IU/l)	16.8±9.01	14.8±9.30
White blood cells/μl	5,909±1,819	5,276±1,505
G0F/G2F ratio	1.10±0.68	1.07±0.55

(10 males and 16 females, aged 42.5±16.9 years) who underwent simultaneous medical check-ups as pairs between 1984 and 1994 were enrolled in this study. All the participants were healthy. Written informed consent was obtained from each subject and the study protocol was approved by the Ethics Committee of Osaka University. We also randomly selected unrelated pairs from this pool of participants and a total of 145 unrelated pairs were analyzed to serve as controls for genetic association.

IgG purification. Serum IgG was purified using protein G sepharose (Amersham Pharmacia Biotech, Buckinghamshire,

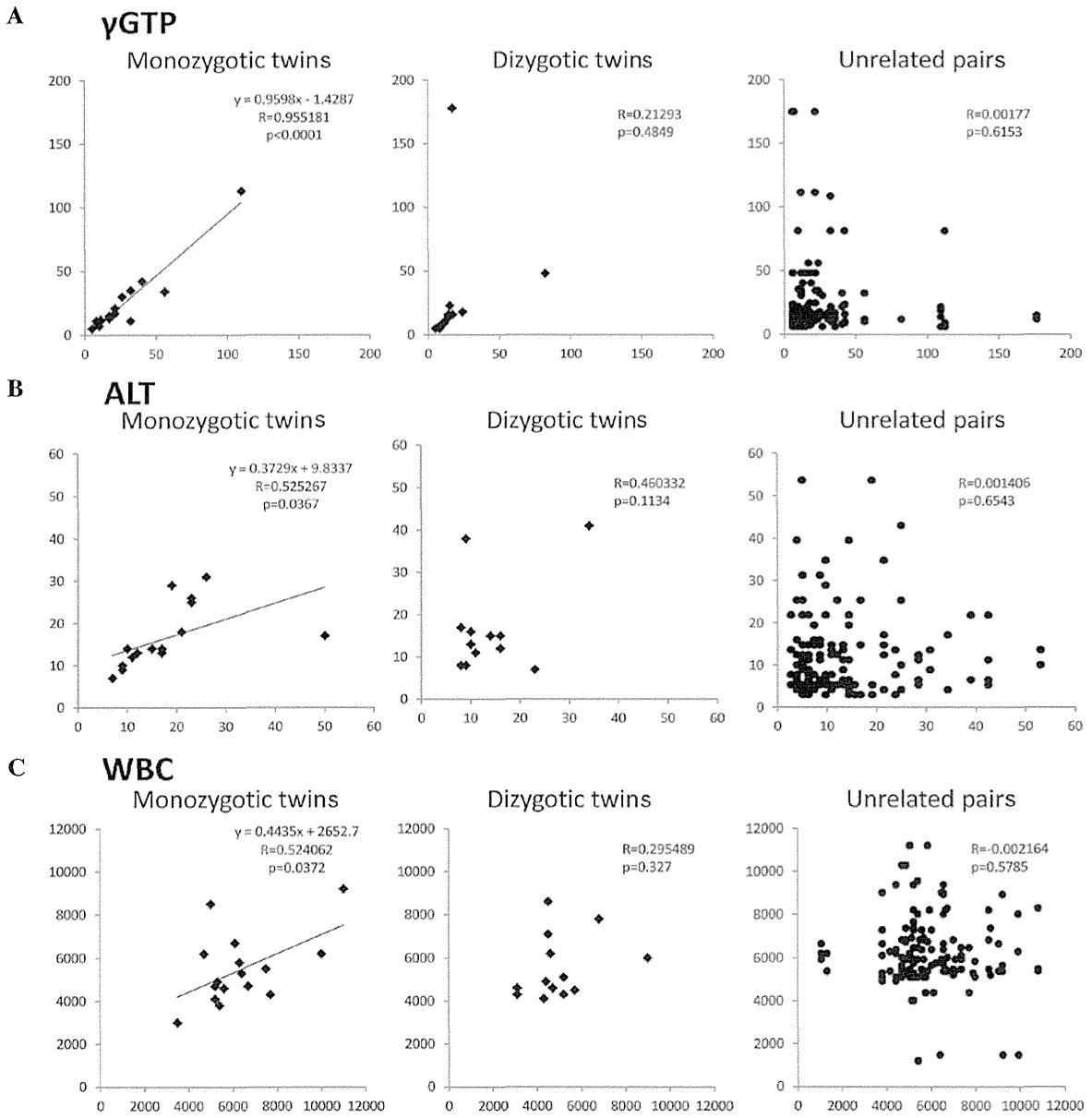

Figure 3. Scatterplots of serum levels of (A) γ-glutamyltranspeptidase (γGTP); (B) alanine aminotransferase (ALT); and (C) white blood cell (WBC) count for monozygotic twins, dizygotic twins and unrelated pairs.

UK). Briefly, serum diluted 1:1 with phosphate-buffered saline (PBS) was loaded onto a protein G sepharose column. The column was subsequently washed with a minimum of 10 column volumes of PBS, followed by the same volume of 10 mM ammonium bicarbonate. Column-bound IgG was eluted using 0.1% trifluoroacetic acid.

Analysis of IgG oligosaccharides. The pyridylaminated N-linked oligosaccharide of IgG was analyzed using reverse-phase high-performance liquid chromatography (HPLC). *N*-linked oligosaccharides were released from serum IgG and labeled with 2-aminopyridine as previously described (7). Briefly, *N*-linked oligosaccharides were released from purified IgG samples following overnight incubation with 0.5 mU glycopeptidase F (Takara Bio, Inc., Sigma, Japan) at 37˚C. The oligosaccharides were then incubated with 0.5 mM ammonium acetate (pH 4.0) for 30 min, lyophilized and labeled with 2-aminopyridine using GlycoTag (Takara Bio, Inc.) according to the manufacturer's instructions. Excess reagent was removed with a cellulose cartridge glycan preparation kit (Takara Bio, Inc.) and the oligosaccharides were incubated with 2 M acetic acid at 80˚C for 2 h to remove sialic acids. The pyridylamino (PA)-oligosaccharides from IgG were analyzed with reverse-phase HPLC (Hitachi High-Technologies Corporation, Tokyo, Japan) using a LaChrom Ultra C18 (2-μm) column (Hitachi High-Technologies Corporation) with 10 mM sodium phosphate (pH 4.4, solvent A) and 10 mM sodium phosphate plus 0.5% 1-butanol (solvent B) at a flow rate of 0.5 ml/min at 40˚C. The glycans were separated with a gradient of 0-50% solvent B for 30 min, followed by 50% solvent B for 10 min. The PA-oligosaccharides were detected using a fluorescence detector (LaChrom Elite, Hitachi) at wavelengths of 320 nm for excitation and 400 nm for emission.

Statistical analysis. The patient characteristics are presented as mean ± SD. The Spearman's rank correlation coefficient was used to assess the correlation of continuous variables within each pair. $P<0.05$ was considered to indicate a statistically significant difference.

Results

IgG oligosaccharide profiles. The normal oligosaccharide structures of neutral human IgG contain 12 major structural variants (Fig. 1A). We analyzed the profiles of IgG neutral oligosaccharides using HPLC in combination with fluorescent labeling of oligosaccharides. In our previous study (7), the G0F/G2F ratio was described as the ratio of the peak height of G0 (agalactosylated IgG) to G2 (fucosylated IgG oligosaccharide group II) (Fig. 1B). Since the majority of IgG oligosaccharides belong to group II, the G0F/G2F ratio represents the total agalactosylation of IgG.

G0F/G2F ratio. We measured the G0F/G2F ratio of IgG oligosaccharides in 32 monozygotic and 26 dizygotic twin pairs. The G0F/G2F ratio was not found to be significantly correlated within monozygotic twin (R=0.215935), dizygotic twin (R=-0.21377), or unrelated pairs (R=-0.0369) (Fig. 2A-C).

Correlations of different markers within pairs. The correlations in serum γ-glutamyltranspeptidase (γGTP) levels were higher within monozygotic twin (R=0.955181) compared to those within dizygotic twin (R=0.21293) and unrelated pairs (R=0.00177) (Fig. 3A). Alanine aminotransferase levels (R=0.525267 for monozygotic, R=0.460332 for dizygotic and R=0.001406 for unrelated pairs) and white blood cell (WBC) count (R=0.524062 for monozygotic, R=0.295489 for dizygotic and R=-0.002164 for unrelated pairs) did not exhibit a strong correlation within twin pairs, although both were found to be significant in monozygotic twin pairs (P=0.0367 and P=0.0372, respectively) (Fig. 3B-C).

Discussion

The agalactosylation of IgG increases with age and is associated with a number of inflammatory diseases. Although the present study included a limited number of twin pairs, the results clearly demonstrated that IgG agalactosylation was not significantly affected by genetics. Of note, γGTP levels were found to be significantly correlated in the 16 pairs of monozygotic twins investigated. Since γGTP levels are often associated with alcohol consumption, this finding suggests that taste and metabolism of alcohol are associated with genetic factors. Although the WBC count is known to vary under different conditions, it was similar between the monozygotic twins in this study. Therefore, compared to WBC, the agalactosylation of IgG appears to be less affected by genetic and more by environmental factors. Furthermore, our studies indicated that twin studies may not a suitable approach to glycobiology investigations.

As the HPLC analysis of IgG oligosaccharides is costly and time-consuming, high-throughput systems, such as ELISA, are required to investigate large numbers of monozygotic/dizygotic twins. Although the lectin-antibody ELISA that we recently developed (8) may be a suitable tool for large-scale analysis of IgG oligosaccharides, it is difficult to evaluate the normal levels of IgG agalactosylation using this method.

To summarize, although the ABO blood type is completely regulated by genetic factors, our results indicated that IgG oligosaccharides are more closely associated with environmental factors and genetic factors do not play a significant role. There are several reports available on the epigenetic regulation of glycosyltransferase genes (8,11) and further studies are required to investigate the epigenetic and environmental factors affecting the agalactosylation of IgG.

References

1. Sox HC Jr and Hood L: Attachment of carbohydrate to the variable region of myeloma immunoglobulin light chains. Proc Natl Acad Sci USA 66: 975-982, 1970.
2. Takahashi N, Ishii I, Ishihara H, *et al*: Comparative structural study of the N-linked oligosaccharides of human normal and pathological immunoglobulin G. Biochemistry 26: 1137-1144, 1987.
3. Mizuochi T, Taniguchi T, Shimizu A, *et al*: Structural and numerical variations of the carbohydrate moiety of immunoglobulin G. J Immunol 129: 2016-2020, 1982.
4. Parekh RB, Dwek RA, Sutton BJ, *et al*: Association of rheumatoid arthritis and primary osteoarthritis with changes in the glycosylation pattern of total serum IgG. Nature 316: 452-457, 1985.
5. Tomana M, Schrohenloher RE, Koopman WJ, *et al*: Abnormal glycosylation of serum IgG from patients with chronic inflammatory diseases. Arthritis Rheum 31: 333-338, 1988.
6. Bond A, Alavi A, Axford JS, *et al*: The relationship between exposed galactose and N-acetylglucosamine residues on IgG in rheumatoid arthritis (RA), juvenile chronic arthritis (JCA) and Sjogren's syndrome (SS). Clin Exp Immunol 105: 99-103, 1996.
7. Shinzaki S, Iijima H, Nakagawa T, *et al*: IgG oligosaccharide alterations are a novel diagnostic marker for disease activity and the clinical course of inflammatory bowel disease. Am J Gastroenterol 103: 1173-1181, 2008.
8. Shinzaki S, Kuroki E, Iijima H, *et al*: Lectin-based immunoassay for aberrant IgG glycosylation as the biomarker for Crohn's disease. Inflamm Bowel Dis 19: 321-331, 2013.
9. Shinzaki S, Iijima H, Fujii H, *et al*: Altered oligosaccharide structures reduce colitis induction in mice defective in β-1,4-galactosyltransferase. Gastroenterology 142: 1172-1182, 2012.
10. Parekh R, Isenberg D, Rook G, *et al*: A comparative analysis of disease-associated changes in the galactosylation of serum IgG. J Autoimmun 2: 101-114, 1989.
11. Kawamura YI, Toyota M, Kawashima R, *et al*: DNA hypermethylation contributes to incomplete synthesis of carbohydrate determinants in gastrointestinal cancer. Gastroenterology 135: 142-151, 2008.

J Gastroenterol (2014) 49:702–714
DOI 10.1007/s00535-013-0813-2

The Japanese Society of Gastroenterology

Expression of *N*-acetylglucosaminyltransferase V in the subserosal layer correlates with postsurgical survival of pathological tumor stage 2 carcinoma of the gallbladder

Kenichiro Onuki · Hiroaki Sugiyama · Kazunori Ishige · Toru Kawamoto · Takehiro Ota · Shunichi Ariizumi · Masayuki Yamato · Shinichi Kadota · Kaoru Takeuchi · Akiko Ishikawa · Masafumi Onodera · Kojiro Onizawa · Masakazu Yamamoto · Eiji Miyoshi · Junichi Shoda

Received: 15 January 2013 / Accepted: 1 April 2013 / Published online: 17 April 2013

Abstract
Background *N*-Acetylglucosaminyltransferase V (GnT-V), an enzyme that catalyzes the β1-6 branching of *N*-acetylglucosamine on asparagine-linked oligosaccharides of cellular proteins, enhances the malignant behaviors of carcinoma cells in experimental models. The aim of this study was to determine clinical significance of GnT-V expression in human pT_2 gallbladder carcinoma with simple in vitro experiments.
Methods Ninety patients with pT_2 gallbladder carcinoma were included for this study. The in vitro and in vivo biological effects of GnT-V were investigated using gallbladder carcinoma cells with variable GnT-V expression levels induced by a small interfering RNA.
Results Of the 90 cases, 57 showed positive staining and the remaining 33 demonstrated negative staining, the subcellular localization in the 57 cases was classified into the granular-type in 31 cases and the diffuse-type in 26 cases. In 76 cases with curative resection, postsurgical survival was significantly poorer in those showing positive staining than in those showing negative staining ($P = 0.028$). In all of the 76 cases, postsurgical recurrence was significantly more frequent in those showing diffuse-type localization than in those showing negative staining. Experimental analyses demonstrated that the down-regulation of GnT-V expression in gallbladder carcinoma cells induced suppression of cell growth in vitro. The expression levels of GnT-V in the cells were highly correlated with the rapid in vivo growth coupled with the enhanced angiogenesis, and the tendency to form liver metastasis.
Conclusions GnT-V expression in the subserosal layer of pT_2 gallbladder carcinoma is correlated with the aggressiveness of the disease.

K. Onuki · T. Kawamoto · T. Ota · S. Ariizumi · M. Yamamoto
Department of Surgery, Institute of Gastroenterology, Tokyo Women's Medical University, Shinjuku-ku, Tokyo, Japan

H. Sugiyama · K. Ishige
Department of Gastroenterology, Division of Biomedical Science, Faculty of Medicine, University of Tsukuba, Tsukuba, Ibaraki, Japan

M. Yamato
Institute of Advanced Biomedical Engineering and Science, Tokyo Women's Medical University, Shinjuku-ku, Tokyo, Japan

S. Kadota · K. Takeuchi
Department of Infection Biology, Division of Biomedical Science, Faculty of Medicine, University of Tsukuba, Tsukuba, Ibaraki, Japan

A. Ishikawa · E. Miyoshi
Division of Health Sciences, Osaka University Graduate School of Medicine, Suita, Osaka, Japan

M. Onodera
Department of Genetics, National Research Institute for Child Health and Development, Setagaya-ku, Tokyo, Japan

K. Onizawa
Department of Oral and Maxillofacial Surgery, Division of Biomedical Science, Faculty of Medicine, University of Tsukuba, Tsukuba, Ibaraki, Japan

J. Shoda (✉)
Medical Science, Division of Clinical Science, Faculty of Medicine, University of Tsukuba, Tsukuba, Ibaraki 305-8575, Japan
e-mail: shodaj@md.tsukuba.ac.jp

Keywords Gallbladder carcinoma · *N*-Acetylglucosaminyltransferase V · Malignant behavior · Postsurgical prognosis · Tumor cell biology

Abbreviations

mAb	Monoclonal antibody
GalNAc-T	*N*-acetylgalactosaminyltransferase
GnT-V	*N*-acetylglucosaminyltransferase
pT	Pathological tumor stage

Introduction

Gallbladder carcinoma has always been associated with a dismal overall prognosis, and this is because the disease is usually detected at an advanced stage [1–5]. The clinical course of gallbladder carcinoma has been thought to depend on the depth of tumor invasion. The 5-year postsurgical survival rates were decreased with tumor invasion: 86–100 % for pathological tumor stage 1 (pT_1) carcinoma, 56–85 % for pT_2 carcinoma, 40–57 % for pT_3 carcinoma, and 9–19 % pT_4 carcinoma [6–8]. Despite a theoretical advantage for pT_2 gallbladder carcinoma (a tumor invading the perimuscular connective tissues but not extending beyond the serosa or into the liver), the prognosis of the disease is not necessarily favorable. The parameters of histopathological malignancies such as lymphatic permeation and venous permeation in the subserosal layer are not correlated with either the mode of recurrence or postsurgical prognosis of pT_2 gallbladder carcinoma [9]. These findings are attributed to various mechanisms in which pT_2 gallbladder carcinoma progresses and to the fact that prognostic factors affecting the progression of less-advanced lesions such as pT_2 gallbladder carcinoma have not been fully elucidated.

Recent advances in glycomics have revealed the scope and scale of the functional roles of oligosaccharides and their effect on human diseases [10]. It is a well-known fact that oligosaccharide structures are dramatically changed in carcinogenesis including malignant transformation. Oligosaccharides are synthesized by a set of several glycosyltransferases, whose genes are approximately 1 % of the human genome. *N*-Acetylglucosaminyltransferase V (GnT-V) is one of the most important among several kinds of glycosyltransferases, which are enzymes involved in carcinogenesis and tumor metastasis [11–13]. GnT-V is involved in the synthesis of β1-6 GlcNAc branching formation on *N*-glycans. A study of GnT-V-deficient mice clearly showed that GnT-V was essential for tumor growth and metastasis [14]. The mechanisms underlying how GnT-V regulates tumor metastasis involve the up-regulation of signaling of many growth factor receptors on the cell surface by suppressing their endocytosis [15], the enhancement of certain kinds of protease activity [16], and the stimulation of angiogenesis as a co-factor [17]. However, immunohistochemical studies of GnT-V showed that GnT-V expression is correlated with poor prognosis of certain kinds of cancer [18, 19], but inversely correlated with other types of cancers [20, 21]. This discrepancy might be dependent on whether or not cancer cells have target proteins of GnT-V or a protease involved in GnT-V cleavage. Although GnT-V has been shown to induce tumor angiogenesis by at least 2 different pathways [16, 17] as well as growth of tumor cells through the up-regulation of growth factor receptors [15], combination studies of clinical and experimental aspects have not yet been performed. Furthermore, pathological investigation of GnT-V products showed that aberrant localization of glycoproteins bearing β1-6 GlcNAc branching is a sign of poor prognosis in melanoma cells [22].

In this retrospective analysis, the immunohistochemical expression of GnT-V was investigated in formalin-fixed, paraffin-embedded surgical specimens from patients with pT_2 gallbladder carcinoma. In 90 cases of pT_2 gallbladder carcinoma, correlations of GnT-V immunostaining at the deepest invading sites in the subserosal layer, as a predictor of invasive/metastatic potential, with the clinicopathological findings, mode of recurrence, and postsurgical survival were investigated. Furthermore, the biological effects of GnT-V on in vitro and in vivo models were studied using gallbladder carcinoma cells with variable GnT-V expression levels induced by a small interfering RNA (siRNA).

Materials and methods

Patients

Specimens from 186 patients (20 normal gallbladder, 19 gallbladder stones, 17 pT_1 gallbladder carcinoma, 90 pT_2 gallbladder carcinoma, 20 pT_3 gallbladder carcinoma and 20 pT_4 gallbladder carcinoma) were included in this study. In the 90 patients with pT_2 gallbladder carcinoma (40 men and 50 women), 76 were curatively resected with a free surgical margin. The mean age of the patients was 67 years (range, 36–83 years). The patients were diagnosed as having gallbladder carcinoma and underwent surgery between 1983 and 2008 in the Department of Surgery, Institute of Gastroenterology, Tokyo Women's Medical University Hospital. Gallbladder carcinoma was diagnosed on the basis of histological findings and classified according to the Tumor-Node-Metastasis classification of the American Joint Committee on Cancer [23]. According to the institutional surgical treatment strategy for pT_2 gallbladder carcinoma, simple cholecystectomy was performed

in 50 patients, cholecystectomy combined with bile duct resection in 9 patients, cholecystectomy combined with bile duct resection and hepatic resection in 12 patients, cholecystectomy combined with bile duct resection and pancreatoduodenectomy in 10 patients, and cholecystectomy combined with pancreatoduodenectomy together with bile duct resection and hepatic resection in 9 patients. Histological examination revealed that all cases of pT_2 gallbladder carcinoma had neither hepatic infiltration nor invasion into the hepatoduodenal ligament.

The follow-up periods until February 2008 ranged from 2.3 to 241.9 months (median time 64 months). Of the 76 patients who had undergone the curative resection with a free surgical margin, 60 were alive as of May 2008, 13 had died from peritoneal dissemination, distant organ metastasis, lymph nodes metastasis and/or local recurrence, and 3 had died from other diseases (cerebral infarction in 1, pseudomixoma in 1, and pneumonia in 1). The latter 3 patients were treated as lost cases.

Cell lines and culture conditions

The gallbladder carcinoma cell lines Mz-ChA-1 and Mz-ChA-2 [24] were obtained from Dr. Alexander Kruth (Johaness-Gutenberg University, Mainz, Germany). The gallbladder carcinoma cell lines TGBC-1-TKB, TGBC-2-TKB, and TGBC-44-TKB (TG44) [25] were obtained from Dr. Takeshi Todoroki (University of Tsukuba, Ibaraki, Japan). The cells were maintained in Dulbecco's modified Eagle's medium containing 10 % heat-inactivated fetal calf serum (Hyclone Laboratories Inc., Logan, UT, USA) in a humidified atmosphere with 5 % carbon dioxide at 37 °C.

Immunoblot analysis of GnT-V

Immunoblot analysis of GnT-V was performed using the lysates of either frozen tissue specimens or cultured cells as described previously [26]. In brief, after 20–30 μg of proteins were electrophoresed on 10 % SDS-PAGE, and then transferred onto a polyvinylidine difluoride (PVDF) membrane. The membranes were incubated overnight in 2 % bovine serum albumin (BSA) in phosphate buffered saline (PBS) at 4 °C and then mixed with a mAb against GnT-V 24D11 (Fuji-revio, Tokyo, Japan) diluted in 2 % BSA (1:500) for 2 h. Each membrane was again probed with a mAb against β-actin (Sigma-Aldrich Co., St. Louis, MO, USA) diluted in 2 % BSA (1:1000). After washing with PBS, the membranes were incubated with goat anti-rabbit or anti-mouse IgG labeled with horseradish peroxidase (Zymed Laboratories Inc., San Francisco, CA, USA) for 40 min. The membranes were then washed with PBS and treated using enhanced chemiluminescence (ECL) (Amersham, Buckinghamshire, UK) to visualize bound antibodies.

Lectin blot analysis

For lectin blot analysis, the membranes were blocked with 3 % BSA in TBST, followed by incubation with 10 μg/ml biotinylated L_4-PHA lectin (Seikagaku Corp., Tokyo, Japan). Reactive bands were detected using the ECL system.

Immunostaining of GnT-V and CD31

Gallbladder carcinoma tissues that had been preserved in 10 % formalin and then embedded in paraffin were serially sectioned at 2 μm thickness, mounted on silane-coated slides, and deparaffinized. The slides were immersed for 20 min in 0.3 % hydrogen peroxide in methanol to deplete endogenous peroxidase. After washing with PBS, the slides were incubated with a protein blocking agent for 5 min at room temperature in a humidity chamber. The slides were then stained by the indirect immunoperoxidase method using an anti-GnT-V antibody, 22G12 (Fuji-revio, Tokyo, Japan) at a 1:3000 dilution rate. A negative control was made using BSA instead of the mAb. Detail procedure was described previously [18].

Evaluation of sections was performed by a single pathologist who was blinded to the clinical characteristics and pathological grade of response. The total number of cancerous epithelia in each section was evaluated. The immunohistochemical localization of GnT-V was classified into the granular-type and diffuse-type based on the predominant subcellular distribution: the granular-type was defined as GnT-V showing granular staining and being restricted predominantly in the supranuclear area of the cancerous epithelia; the diffuse-type was defined as GnT-V showing no granular staining and being found in the cytoplasm of the cancerous epithelia. GnT-V localization was judged to be either the granular or diffuse type when 50 % of the total number of cancerous epithelia in each section showed granular-type or diffuse-type subcellular distribution, and the localization was examined in both the mucosal or proper muscle layers (surface site) and the subserosal layer (invading site).

To investigate the association of GnT-V expression with tumor angiogenesis in gallbladder carcinoma, microvessels (capillaries and venules) around the cancerous epithelia were counted. Microvessels were highlighted by staining the endothelial cells with mAb raised against CD31 (Abcam, Cambridge, MA, USA) according to the standard immunoperoxidase technique [27]. Areas representative of the invasive component of the carcinoma were selected from the hematoxylin and eosin-stained sections. Microvessel density was assessed without prior knowledge of GnT-V staining. Microvessels were carefully counted (per 100× field) and the microvessel density in each field was

defined as the mean number of microvessels containing high levels of CD31-stained microvessels.

Construction of GnT-V knockdown gallbladder carcinoma cells

Suppression of GnT-V expression in TG44 cells was achieved using a siRNA duplex. A retrovirus, which encodes a siRNA against GnT-V, was obtained from Dr. Naoyuki Taniguchi [28]. TG44 cells were infected with the retrovirus, and then the cells were selected with 0.8 mg/ml G418 for 2–3 weeks. Stable GnT-V knockdown TG44 cells were cloned and confirmed by immunoblot analysis as described earlier.

Construction of gallbladder carcinoma cells expressing luciferase

To establish TG44 cells expressing luciferase (TG44-luc), TG44 cells were infected with a retrovirus encoding luciferase and enhanced green fluorescent protein (EGFP), which was generated by Dr. Masafumi Onodera [29, 30], and the resulting cells were cultured for 3–7 days. Cell lysates were prepared and subjected to luciferase assay (Promega, Madison, WI) to confirm luciferase expression.

Enzyme assay of GnT-V

GnT-V enzyme activity was determined as described previously [31].

Cell viability assay

The in vitro effects of GnT-V on the growth viability of gallbladder carcinoma cells were determined by a cell viability assay using a WST-8 reduction assay kit (Dojin Laboratories, Tokyo, Japan) according to the manufacturer's instructions. Gallbladder carcinoma cells were plated at 1×10^3 cells per well in 96-well microtiter plates. WST-8 was added and cell viability was determined by reading optical density values from a microplate reader at an absorption wavelength of 450 nm. All assays were performed twice. The IC_{50} value, at which 50 % cell growth inhibition compared with that of the dimethyl sulfoxide control was obtained, was calculated.

Subcutaneous xenografted tumor model

Four-week-old female BALB/c nu/nu athymic mice (Sankyo Labo Service, Tokyo, Japan) were quarantined for 1 week. The animal experiment protocols were approved by the Institutional Animal Care and Use Committee of Tokyo Women's Medical University. A gallbladder carcinoma xenograft model was prepared by injecting 1×10^7 TG44 cells induced by a siRNA in 100 μl of PBS into the left flank of each mouse. Tumor size was measured using a Vernier caliper and tumor volume was calculated as $0.5 \times \text{longest diameter} \times \text{width}^2$.

Persplenic hepatometastatic tumor model

A persplenic hepatometastatic tumor model injected with 2×10^6 TG44-luc cells induced by a siRNA was prepared as previously described [32]. In the mice, photon counting was conducted once a week. Bioluminescence images were used to monitor the dynamics of intrahepatic tumor growth. Immediately before imaging, 150 mg/kg D-luciferin (Alameda, CA, USA) was intraperitoneally administered to the mice. After 15 min, photons from whole bodies were counted using the IVIS imaging system (Xenogen, CA, USA) in accordance with the manufacturer's instructions. Total flux (photons/sec) of emitted light was used as a measure of the relative number of viable tumor cells in the peritoneal tumor. Data were analyzed using LIVING IMAGE 3.0 software (Xenogen).

Statistical analysis

Values are presented as mean ± SE (standard error). Statistical evaluations of data were analyzed using the χ^2 test for independence test, Student's t test, and one-way ANOVA followed by the Tukey–Kramer test. Survival curves of the postsurgical outcome of the 76 curative resection cases of pT_2 gallbladder carcinoma and animals in the hepatometastatic tumor model were analyzed using the Kaplan–Meier method. Differences in the survival of the 76 curative resection cases of pT_2 gallbladder carcinoma and animals in the subgroups were analyzed by the log-rank test. Several clinicopathological factors were subjected to multivariate regression analysis using the Cox proportional hazards regression model. Cox regression was accessed using the statistical program SPSS. A P value of less than 0.05 was considered to indicate a statistically significant difference.

Results

Immunoblot analysis of GnT-V in gallbladder carcinoma tissues

GnT-V protein was included in the lysates of the specimens of gallbladder carcinomas and normal gallbladders (Fig. 1a). GnT-V protein levels were increased at varying degrees in the tissue specimens of pT_1–pT_3 gallbladder carcinomas compared with the GnT-V protein levels in the specimens of normal gallbladders (Fig. 1a).

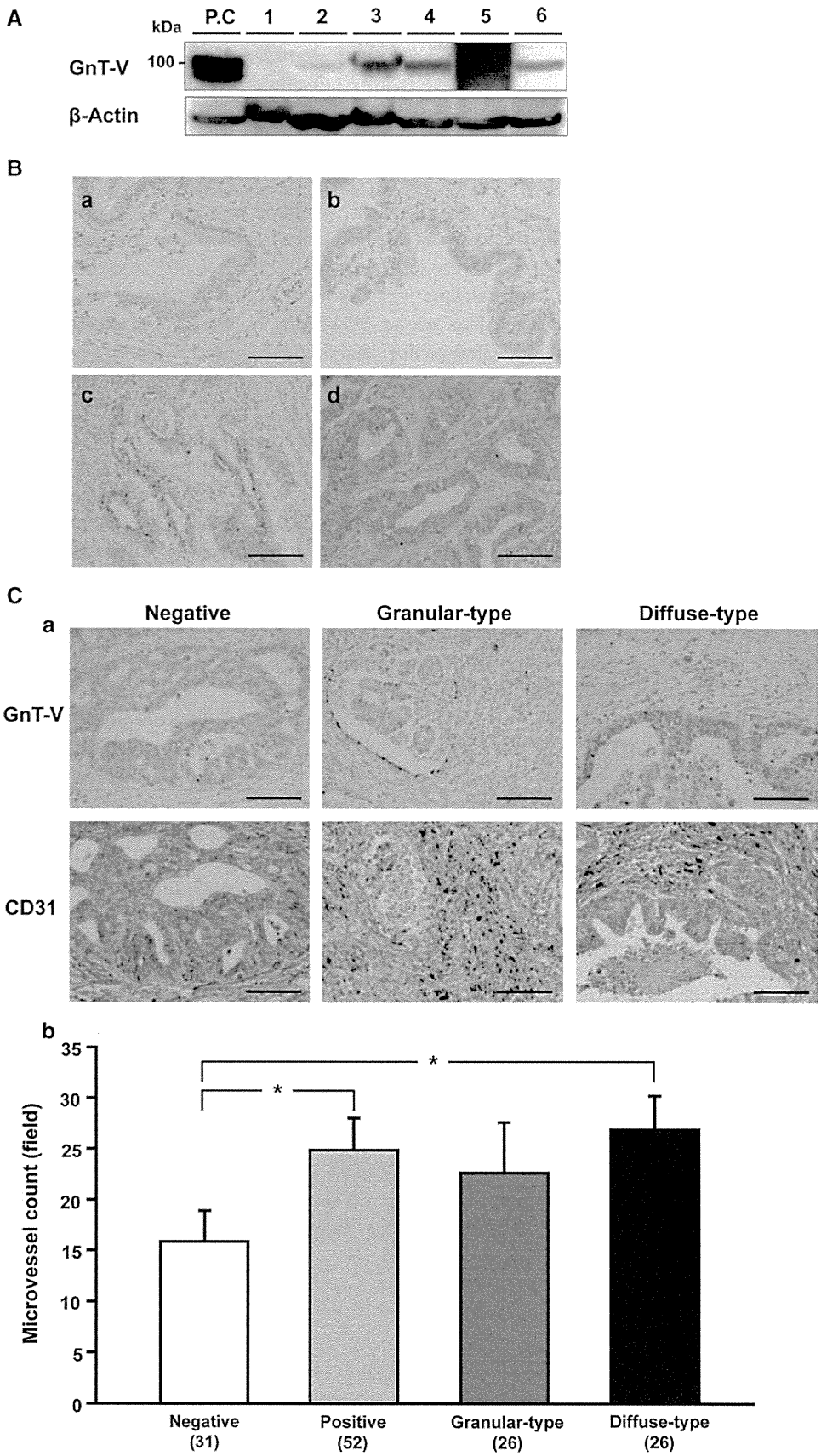

Fig. 1 **A** Immunoblot analysis of GnT-V in normal gallbladders and gallbladder carcinoma tissues. Protein was normalized to β-actin. GnT-V transfected WiDr cells (a colon carcinoma cell line) was used as a positive control (P.C). *Lanes 1* and *2* lysates of normal gallbladders, *Lane 3* lysate of pT_1 gallbladder carcinoma tissue, *Lanes 4* and *5* lysates of pT_2 gallbladder carcinoma tissues, *Lane 6* lysate of pT_3 gallbladder carcinoma tissue. **B** Immunohistochemical localization of GnT-V in the epithelia of normal gallbladder (**a**), in those of gallbladder associated with gallstones (**b**), and those of pT_2 gallbladder carcinoma (**c**, **d**). GnT-V localization was mostly the granular-type for normal epithelia and noncancerous pathological epithelia of the gallbladders. However, GnT-V localization was heterogeneous: granular- (**c**) and diffuse- (**d**) types for the cancerous epithelia of gallbladder carcinoma. *Bars* 100 μm. **C** Immunostainings of CD31 and GnT-V in the epithelia of pT_2 gallbladder carcinoma. *Bars* 100 μm (**a**). Quantification of data of microvessel density in tissue sections. A tissue section was prepared from each case of gallbladder carcinoma patients. Five photographs were taken for each tissue section and analyzed. Microvessels showing CD31 immunoreactivity was counted. Microvessel density for each of the 5 photographs of the tissue section was averaged. The averaged densities were compared in terms of GnT-V expression levels (**b**). *Columns* and *bars* represent means and SE of the microvessel densities in each group, respectively. Significant differences between the 2 groups are indicated by $*P < 0.05$

Immunohistochemical staining and localization of GnT-V in gallbladder carcinoma

The immunohistochemical staining and localization of GnT-V in pT_1-pT_4 gallbladder carcinomas, those in normal gallbladders and those in gallbladders associated with gallstones, were investigated (Table 1). The expression rate of GnT-V was significantly higher in pT_1–pT_4 gallbladder carcinomas (69 %) and gallbladders associated with gallstones (63 %) than in normal gallbladders (5 %). The expression rate of GnT-V was not significantly different from pT_1 gallbladder carcinoma in the early stage to pT_3 and pT_4 gallbladder carcinomas in the advanced stage. Consistent with the increased GnT-V protein levels detected by immunoblot analysis (Fig. 1a), GnT-V immunostaining was found to be more intense in the cancerous epithelia than in the normal epithelia of the gallbladders (Fig. 1b). GnT-V localization was heterogeneous in gallbladder carcinomas with the granular- or diffuse-type of subcellular distribution, in contrast with GnT-V localizations in normal gallbladders and gallbladders associated with gallstones, which were solely the granular-type (Fig. 1b). Notably, the proportion of the diffuse-type localization of GnT-V at the deepest invading sites was increased significantly in pT_2, pT_3, and pT_4 gallbladder carcinomas compared with the proportion in the noncancerous epithelia.

Moreover, CD31 immunostaining was performed in 83 cases of pT_2 gallbladder carcinoma and the microvessels around the cancerous epithelia were counted to investigate the association of GnT-V expression levels with tumor angiogenesis (Fig. 1c). The number of microvessels was significantly higher in 52 cases with positive expression (25 ± 3 per $100 \times$ power field) than in 31 cases with negative expression (16 ± 3). Moreover, in terms of GnT-V localization type, the numbers of microvessels were 23 ± 5 in 26 cases in the granular-type locatization group and 27 ± 3 in 26 cases in the diffuse-type localization group. The number of microvessels was significantly higher in the diffuse-type localization group than in the negative expression group.

Table 1 The immunohistochemical localization of GnT-V in normal epithelia and that in gallbladder stones and pT_1–pT_4 gallbladder carcinomas

	Negative	Positive	Localization type	
			Granular	Diffuse
Normal ($n = 20$)	19	1	1	0
Gallbladder stone ($n = 19$)	7	12	12	0
Gallbladder carcinoma ($n = 147$) (pT_1–pT_4)	46	101[a]	55	46[b]
pT_1 ($n = 17$)	5	12[a]	9	3
pT_2 ($n = 90$)	33	57[a]	31	26[b]
Curative resection case ($n = 76$)	30	46	27	19
Non-curative resection case ($n = 14$)	3	11	4	7
pT_3 ($n = 20$)	3	17[a]	10	7[b]
pT_4 ($n = 20$)	5	15[a]	5	10[b,c]

[a] $P < 0.01$, significantly different from normal epithelia

[b] $P < 0.01$, significantly different from gallbladders associated with gallstones

[c] $P < 0.05$, significantly different from pT_1 carcinoma

Relationship between clinical findings and GnT-V expression in patients with pT_2 gallbladder carcinoma

The 76 curative resection cases of pT_2 gallbladder carcinoma were divided into 2 groups based on GnT-V staining at the deepest invading sites in the subserosal layer. A comparison of positive and negative groups was made with special reference to the clinical features, that is, gender, age, gallstones, tumor size, preoperative serum CEA, and CA19-9 (Table 2). The results revealed no significant differences in the clinical features between the 2 groups. A comparison was also made in terms of GnT-V localization (Table 2). The results showed no significant differences in the clinical features between the 2 groups.

Relationship between parameters of pathological malignancies and GnT-V expression in patients with pT_2 gallbladder carcinoma

A comparison of positive and negative groups was also made with special reference to the parameters of pathological malignancies, that is, histological grade, lymphatic permeation, venous permeation, and lymph node metastasis (Table 3). The results revealed no significant differences in the parameters of pathological malignancies between the 2 groups. A comparison was also made in terms of GnT-V localization (Table 3). The results showed no significant differences in the parameters of pathological malignancies between the 2 groups.

Relationship between mode of recurrence in patients with pT_2 gallbladder carcinoma and GnT-V expression in the specimens

The postsurgical recurrent mode in 76 curative resection cases of pT_2 gallbladder carcinoma was compared in terms of GnT-V expression (Table 4). Of the 46 cases showing positive staining, 7 had distant organs metastasis and 6 had lymph node metastasis. In contrast, of the 30 cases showing negative staining, 1 had peritoneal dissemination and 1 had

Table 2 Relationship between clinical findings and immunohistochemical expression of GnT-V in curative resection cases of pT2 gallbladder carcinoma

	Negative	Positive	Localization type	
			Granular	Diffuse
Number	30	46	27	19
Gender (M/F)	11/19	20/26	10/17	10/9
Age	65 ± 12	68.2 ± 9.8	67.6 ± 9	68.9 ± 10
Gallstones (±)	14/16	24/22	14/13	10/9
Tumor size (mm)	32.5 ± 18	32.1 ± 20.5	30.9 ± 18.7	33.5 ± 22.6
CEA	4.17 ± 8.2	4.37 ± 6.6	3.99 ± 6.77	4.65 ± 6.91
CA19-9	34.2 ± 49.3	414.9 ± 1228	686.7 ± 1640	29.1 ± 31.9

Table 3 Correlation between histopathological findings and immunohistochemical localization of GnT-V in pT_2 gallbladder carcinomas

	Negative	Positive	Localization type	
			Granular	Diffuse
Number	30	46	27	19
Histlogical grade				
G1	17	33	20	13
G2-4	13	13	7	6
Lymphatic permeation				
+	18	34	19	15
−	12	12	8	4
Venous permeation				
+	16	18	12	6
−	14	28	15	13
Lymph node metastasis				
+	11	19	10	9
−	19	27	17	10

There is no significant difference between immunohistochemical localization of GnT-V and histopathological findings of the 76 curative cases of pT_2 gallbladder carcinomas

distant organs metastasis. Note that in pT_2 gallbladder carcinoma, postsurgical recurrence in distant organs tended to be more frequent in patients in the positive staining group (15 %) than in patients in the negative staining group (3 %). Moreover, postsurgical recurrence in distant organs was found to be significantly more frequent in the diffuse-type localization group (26 %) than in the negative staining group (3 %; $P < 0.05$). Therefore, the diffuse-type localization of GnT-V at the deepest invading sites may be an important biological predictor of postsurgical recurrence of pT_2 gallbladder carcinoma.

Relationship between synchronous metastasis in the liver of patients with pT_2, pT_3 or pT_4 gallbladder carcinoma and GnT-V expression in the specimens

GnT-V expression at the deepest invading sites was compared in pT_2, pT_3 and pT_4 gallbladder carcinoma patients with synchronous liver metastasis at the time of surgery and those without metastasis (Table 5). Of 130 patients, 14 had synchronous liver metastasis and the remaining 116 had none. Synchronous liver metastasis was found to be significantly more frequent in the diffuse-type localization group (19 %) than in the negative staining group (5 %; $P < 0.05$).

Relationship between postsurgical survival of patients with pT_2 gallbladder carcinoma and GnT-V expression in the specimens

The overall postsurgical survival rate in the 76 patients with pT_2 gallbladder carcinoma was compared in terms of GnT-V expression (Fig. 2a). The survival rate of patients in the

Table 4 Postsurgical recurrent modes in pT_2 gallbladder carcinoma

Immunohistochemical localization of GnT-V	Total	Peritoneal dissemination	Distant organs[a]	Lymph Nodes	Local recurrence
Negative ($n = 30$)	5	1	1	0	3
Positive ($n = 46$)	16	0	7	6[d]	3
Granular-type ($n = 27$)	7	0	2	4	1
Diffuse-type ($n = 19$)	9[b]	0	5[c]	2	2

[a] Distant organs included the liver in 6 patients, lung in 1 patient and bone in 1 patient

[b] $P < 0.05$, significantly different from negative staining group

[c] $P < 0.05$, significantly different from negative staining group

[d] $P < 0.05$, significantly different from negative staining group